amt-2020-240

Thank you for reviewing the manuscript and providing constructive comments. We have made edits to the manuscript incorporated with your suggestions. Reviewers' comments are shown in black, our response to each comment is shown in blue, and changes to the manuscript are shown in red.

Reviewer #1:
There are some interesting and useful components of this manuscript related to differences in ground-based and airborne wind retrieval methods. The writing and organization are clear, for the most part. However, there are several major concerns with the paper as listed below that will take a significant amount of time to address. I therefore recommend that the paper be declined and re-submitted once these issues are addressed.

Major:
(1) The total error in the radar comparisons is a summation of instrument effects (e.g., signal-to-noise ratio), sampling effects (e.g., gaps in data coverage, spatial/temporal resolution) and algorithm effects (e.g., geometry, approximations, solution method). The comparisons between dual Doppler and single Doppler retrievals for WV#0 tangential winds have some differences in the eyewall region (especially pass 4) that appear to be due to differences in the GVTD method (algorithm effect). The authors are trying to isolate the effects of the "steady-state" assumption (sampling effect) in airborne radar analysis by comparing WV#1 and WV#2 tangential winds from dual Doppler and single Doppler retrievals. However, it is not at all clear how much of the differences the authors are seeing are due to instrument effects, algorithm effects or other sampling effects. The WV#1 and WV#2 tangential winds should have larger errors due to algorithm effects when compared to the WV#0 tangential winds. This makes it very difficult or impossible to isolate the effects of just the steady-state assumption and thus the conclusions from this analysis are uncertain. The authors need to isolate these effects through some type of simulated analysis in order to make definitive conclusions.

Thank you for the comment. We agree we did not adequately discuss the total error in the radar comparisons in the manuscript. Additional discussion, previous literature reviews of the sources of error, and a new figure supporting our claim that the sampling error is a large contributor to the differences have been added to the manuscript. The instrument and algorithm errors are relatively small, but the sampling effect, particularly a long period of data collection for the airborne Doppler radar observation, could result in aliasing in the analysis with the steady-state assumption in a snapshot. To provide further support for this hypothesis, we performed an idealized experiment with a rotating wavenumber 2 tangential wind sampled by an aircraft with a realistic scanning strategy. We 'fly' a simulated aircraft track through an idealized vortex in a typical straight-line flight track during P3 operational reconnaissance. A wavenumber 2 Rankine edge wave propagating around 20 km RMW at 1/2 V_{max} is sampled by the simulated flight, which takes 22 minutes to finish a 160 km flight leg.

The new Figure 8 in the manuscript, reproduced here (Fig. 1), shows the derived tangential wind for a rotating wavenumber 2 during the flight pass. In this idealized experiment, we have minimized all the other errors such that a steady-state vortex is retrieved nearly

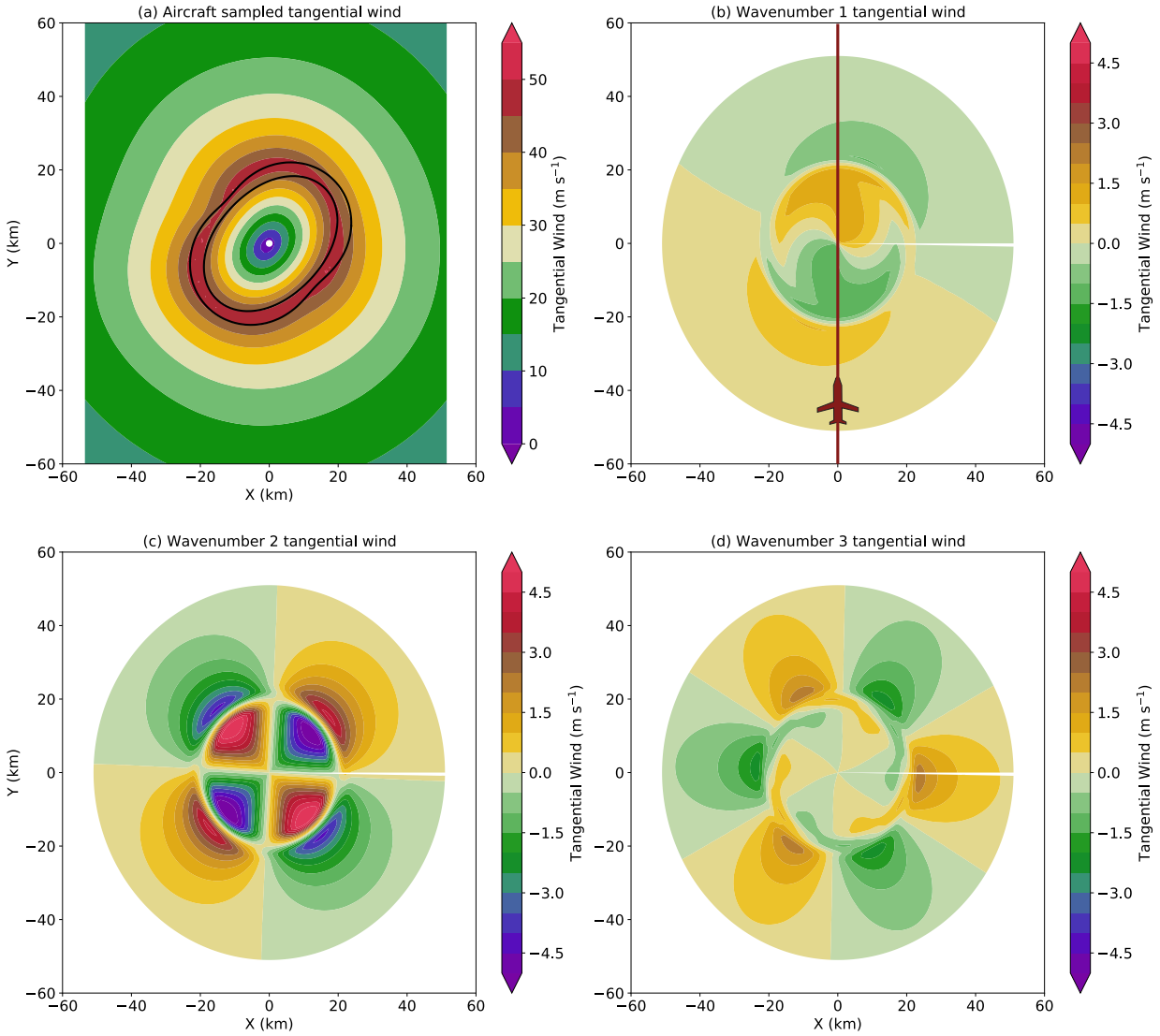

Figure 1: (a) Idealized dual-Doppler tangential wind speed retrieved from a straight flight pass through propagating wavenumber two asymmetry (color in m s^{-1}) and 50 m s^{-1} contour of time-averaged wavenumber two in black. The initial phase of the propagating wavenumber 2 tangential wind is oriented from east to west and final phase is from north to south. (b) Wavenumber 1 plus aircraft flight track from south to north, (c) Wavenumber 2, and (d) Wavenumber 3 tangential wind components retrieved by the Fourier decomposition of the tangential wind field shown in panel (a).

exactly. The distorted tangential wind field suggests temporal aliasing from the extended sampling period of the aircraft pass due to the propagation of the wavenumber 2 asymmetry. Although we only prescribed a propagating wavenumber 2 Rankine wave in the experiment, both wavenumber 1 and 3 components are with non-trivial amplitude. Based on comments from another reviewer, we have also clarified that there are in effect two different types of sampling errors that arise from the steady state assumption – the first is due to the time lag between fore and aft beams, and the second is due to the length of time used to composite the multi-Doppler into a single snapshot. While both produce some errors, the latter is more consequential when considering low-wavenumber asymmetries since it takes longer to capture the larger scale structure, resulting in evolution over the flight pass. This idealized experiment shows that the steady-state assumption of one straight flight leg to

synthesize the data into one snapshot with the presence of rapidly evolving features could result in temporal aliasing and result in potential misinterpretation of the asymmetric flow field. Additional errors are possible from instrument and algorithm effects, and this has now been clarified in the revised manuscript.

We have included the discussion on different sources of error here for reference. Please see the revised manuscript for the full description of the new Figure 8.

Although dual-Doppler observations can be used to assess snapshots of high resolution kinematic and convective structure, airborne reconnaissance and research missions are rare events in most of the countries impacted by TCs. The three-dimensional airflow structure can also be retrieved from the dual-Doppler observations when the system is detected by two ground-based radars. General sources of error in the inter-comparison of ground-based and airborne dual-Doppler observations include instrument effects, algorithm effects, and sampling effects [Hildebrand and Mueller, 1985]. Instrument effects include the effects of attenuation and signal-to-noise ratio that could be caused by the radar processor design or measurement technique. These effects are likely to be most influential with marginal signal-to-noise, but random velocity errors up to 1 m s^{-1} are possible with many radar designs, including airborne radars [Hildebrand et al., 1994]. Algorithm effects include the effects of the interpolation to the Cartesian grid, multi-Doppler geometry, the solution method and its associated assumptions, and the derivation of the vertical velocities. Sampling effects include the effects of data spacing and density, geometry of flight tracks, temporal changes in the storm, advection, and data collection period. One of the long-lasting problems is the length of time required for each flight leg with airborne Doppler radar [Ray and Stephenson, 1990].The temporal effects can degrade the analysis if the data collection takes too long. [Jorgensen et al., 1983] quantitatively compared the wind fields of homogeneous precipitation derived from the two pseudo-orthogonal flight legs and two ground-based dual-Doppler observations. Their measurements showed agreement in the horizontal wind fields, but small discrepancies in the vertical velocities about 0.5 - 1 m s^{-1} for the airborne system and about 0.2 m s^{-1} for the ground-based system. The discrepancy was attributed to uncertainties in the pointing angle of the airborne system and a long data collection period.

(2) Regarding the improved GVTD method: the authors have done a thorough analysis of the impacts of storm motion on the ground-based retrieval. I think this analysis is useful for the community. However, I think the revised method only makes minor improvements on the errors in the retrieved mean tangential winds, but the authors have overstated their importance at several places in the paper, including the abstract. Thus, the tone of the paper needs to be revised in several places and more details are found in the additional comments section.

Thank you for the comment, and we have revised the tone throughout the paper. As the reviewer has mentioned above, the error sources can come from instrument effects, sampling effects, and algorithm effects. While the improvement is small, as discussed in Jorgensen et al. 1983 , the accumulation of different sources of errors can contribute to a large amount, such that a minimization of all the known errors is needed. The errors from the contribution of storm motion could be large if the storm moves fast or when the storm tracks closer to the radar (R_T is small). The estimated storm motion of Hurricane Matthew (2016) is 8.4, 8.2, 3.8, 6.1 m s^{-1} on pass 1 to 4, respectively, and Matthew is about 200 km away from the radar. Therefore, the averaged RMSE of the four passes shown in the manuscript is

not that large, but we think that the improvement on the errors from the improved GVTD technique are important and contribute to the reduction in total error. The accuracy of the estimated hurricane intensity is important when the storm moves inland or closer to the radar observation range. We have modified the tone of the description for the results, with two examples given here:

Abstract: A comparison between the two techniques shows that the axisymmetric tangential winds are generally comparable between the two techniques, and the improved GVTD technique improves the accuracy of the retrieval.

While it is a relatively small reduction in the RMS difference in the current case, the statistically significant difference in this algorithm error contributes to an overall reduction in the total error from instrument, algorithm, and sampling contributions.

Conclusion: A comparison between the two techniques shows that the retrieved axisymmetric (wavenumber 0) component of tangential winds are generally comparable between the two techniques, and the improved GVTD technique improves the accuracy of the retrieval.

(3) Regarding the radar analysis with P3 data: the authors have used a grid spacing of 1 km in the horizontal direction. With the fore/aft scanning technique and antenna rotation rate of 10 RPM in 2016 data, there is really no way to arrive at 1 km horizontal grid spacing for the wind analysis. The spacing of radials is on the order of 1.4 km so 2 km horizontal grid spacing is about as good as it gets. The authors would need to redo their analysis with 2 km grid spacing and scale the ground-based analysis accordingly. This could change some of the results. In addition, the storm core passed through on the far edge of the ground-based radar coverage when the P3 data was compared. The beam spread at this far range is substantial and the grid spacing of the ground-based analysis of 1 km in the horizontal and 0.5 km in the vertical may not accurately reflect the pulse volume. Some discussion and/or analysis of this effect is also needed.

Thank you for the comment. We realize we neglected to describe the fact that low-pass filtering was applied to the P-3 analysis to ensure that the resolved scales were in fact consistent with the data spacing, but this has now been corrected in the revised manuscript. As shown by Koch et al. 1983 and others, we believe the grid spacing should be smaller than the data spacing in order to accurately resolve the maximum spatial scales available for the given sampling. In SAMURAI, the 'grid spacing' is actually a 'nodal-spacing' since the resolved wind field is a function composed of finite elements. The nodal-spacing determines the minimum spatial scale resolved by the spline function of 2dx. In the current analyses, we use a 4dx Gaussian filter in the horizontal and 2dx filter in the vertical. Therefore, the resolved spatial scales are ~4 km in the horizontal, which is well above both the along-track spacing, radar range volume, and azimuthal beam volume. While the vertical resolution may be a bit fine even after filtering, we focus on the horizontal structure in the paper and feel our analysis accurately resolves the appropriate spatial scales for the given sampling.

A low-pass filtering was applied to the P-3 analysis to ensure that the resolved scales were in fact consistent with the data spacing. The grid spacing should be smaller than the data spacing in order to accurately resolve the maximum spatial scales available for the given sampling [Koch et al., 1983].

(4) Heavy use of NOAA TDR data is used in this study. This data is collected and processed (i.e., level 1 data) by NOAA and HRD. Unfortunately, the authors have not either (1)included a co-author from HRD or (2) made any mention of HRD in the acknowledgements section of the paper. NOAA/HRD has a data policy statement about these kinds of things that requires at the least, an acknowledgement for use of the TDR data. The authors need to rectify this in a re-submission of the paper.

Thank you for the comment and we apologize for the oversight. We have added the acknowledgement of NOAA/HRD, and are very grateful for the data collection efforts of NOAA Aircraft Operations Center and HRD.

We would like to thank NOAA Aircraft Operations Center and the Hurricane Research Division of the Atlantic Oceanographic and Meteorological Laboratory for collecting the airborne tail Doppler radar data used for this study, and the National Weather Service for the ground-based radar data.

Additional:

Lines 10 – 11; "A comparison between the two techniques shows that the axisymmetric tangential winds are generally comparable between the two techniques after the improvements to GVTD retrievals." The comparisons of WV0 tangential winds are generally comparable before the GVTD improvements as well. The improvements don't change the values that much. Sentence needs re-wording.

Thank you for the comment. We have reworded the sentence.

A comparison between the two techniques shows that the axisymmetric tangential winds are generally comparable between the two techniques, and the improved GVTD technique improves the accuracy of the retrieval.

Line 21; don't need measurements from two or more radars if the platform is in motion, such as airborne Doppler radar. Please clarify.

Thank you for the comment. We have clarified the sentence.

In addition to the presence of an airborne Doppler radar with fore/aft capability or multiple radars with sufficient range and geometry around the TC, a steady state assumption during the Doppler radar observation period is required to synthesize the wind fields into one snapshot in time.

Line 25; There are some papers that have analyzed wind retrieval techniques for TCs and with varying platforms. Please cite some of those papers here.

Thank you for the comment. Several references have been added.

Previous studies have shown the intercomparison of dual Doppler wind fields from two orthogonal flight legs and a ground-based two-radar network [Jorgensen et al., 1983], [Hildebrand and Mueller, 1985]. Several other studies have investigated both single and multi-

Doppler techniques for retrieving TC wind fields [Lee et al., 1994, Crum et al., 1998, Reasor et al., 2000, Lee et al., 1999, Jou et al., 2008, Bell et al., 2012], but the strengths and weaknesses of different techniques have not been compared and addressed fully. In this study, ground-based single Doppler and airborne dual Doppler observations simultaneously sampling Hurricane Matthew (2016) are analyzed to provide the first comprehensive comparison between ground-based single and airborne multi-Doppler wind retrieval techniques in a TC.

Line 27; I highly doubt that this is the first study to compare ground-based and airborne wind retrievals. The NOAA ground-based and airborne radars have been around for decades!

Thank you for the comment. We have added several references on these types of comparisons, and clarified that we mean specifically that the comparison between single-Doppler wind retrievals and airborne dual-Doppler has not been conducted. The comparison between ground-based dual Doppler and airborne wind retrievals was done in 1980s to 1990s, but the wind field retrieved by a single Doppler radar observation has not been compared with the airborne dual Doppler observations to our knowledge. Please refer to the previous response for the revised sentences and additional references.

Lines 56 – 57; sentence doesn't read right,"...only a small portion of TC"? Please rewrite.

Thank you for the comment. We have revised the sentence.

Ground-based dual-Doppler radar observations of TCs are usually limited to the observation of storms that happen to develop or move within the domain covered by the radars and extensive radar baselines [Jou et al., 1996].

General comment on the writing; at several places in the paper the word "the" needs to be inserted. Go through the paper again and look for these. Some examples:
Line 96,"...and P3 TDR..." needs a "the" before "P3"
Line 98, "...of KAMX radar..." needs a "the" before "KAMX"

Thank you for the comment. We have gone through the paper and added the missing word.

Line 122, Does this "mean" wind have the hurricane removed?

Thank you for the comment. The mean wind magnitude and direction were derived from the airborne dual Doppler analysis, following the procedure proposed by [Marks et al., 1992]. The storm-relative horizontal wind field (V_r)in a cylindrical coordinate system centered on the storm can be decomposed into:

$$V_r(r,\theta,z) = \bar{V}_r(z) + V'(r,\theta,z) \tag{1}$$

where r is radius, θ is azimuth, z is height, $\bar{V}_r(z)$ is the horizontally averaged wind vector over the radius and azimuth, and $V'(r,\theta,z)$ is the deviation from $\bar{V}_r(z)$. $\bar{V}_r(z)$ can be expressed as:

$$\bar{V}_r(z) = \frac{1}{2\pi}\int_0^{2\pi}\int_0^{r_{max}} V_r(r,\theta,z)drd\theta \tag{2}$$

If the horizontal wind field is from a circular symmetric vortex with no steering flow, $\bar{V}_r(z)$ would be zero. Nevertheless, if the vortex is embedded in the steering flow, the averaged horizontal wind field would equal the mean wind component. Thus, the local wind shear can be approximated by subtraction of the mean wind component at different altitudes. In our study, we calculated the mean wind component averaged from the vortex inner core area within the radius of 60 km.

The mean wind (V_M) is the horizontal average of the environmental flow at each altitude following the procedure proposed by [Marks et al., 1992], which can be used to calculate the vertical wind shear.

Equation (4), The two angles in the second terms on the RHS of (4) should be THETAt, not THETA. This is probably just a typo.

Thank you for the comment. We have corrected the typoes.

$$\begin{aligned} Dcos\theta_d &= Rcos\theta + R_T cos\theta_T \\ Dsin\theta_d &= Rsin\theta + R_T sin\theta_T \end{aligned} \tag{3}$$

Line 150, what is the lowest elevation angle used here and what error does this incur? The method must only work where cos(phi) $\sim$ 1, so lowest scan level only.

Thank you for the comment. Figure 2 shows the radar beam elevations of 0.5° and 0.9° versus the range. The distance between the KAMX radar and the TC center of the four radar volumes corresponding to the four flight passes are highlighted by the vertical lines. Our analysis focuses on the altitude of 4 km, and the four radar volumes at this altitude is constructed by the radar beam below 1° elevation angle. Therefore, the assumption of Vd $\sim$ Vd/cos(ϕ) is applicable.

Plugging Eq. 4 into Eq. 3 and approximating $\hat{V}_d/cos\phi$ with V_d (only valid when the elevation angle is low):

Lines 177 – 179, this assumption is probably only valid above the boundary layer and below the outflow layer. Radial wind asymmetries can be substantial in the boundary layer. Some discussion of this is needed.

Thank you for the comment. We have added the conditions to the assumption.

This closure assumption may not be applicable within the boundary layer or outflow layer where the radial wind asymmetries can be substantial.

Page 8, this entire page could be significantly shortened because the "dynamic" centers are ultimately used, not the GBVTD centers. This can be summarized briefly.

Thank you for the comment. We would like to present the GVTD simplex algorithm which outperforms the GBVTD-simplex algorithm as a reference for future work. The spline fit of

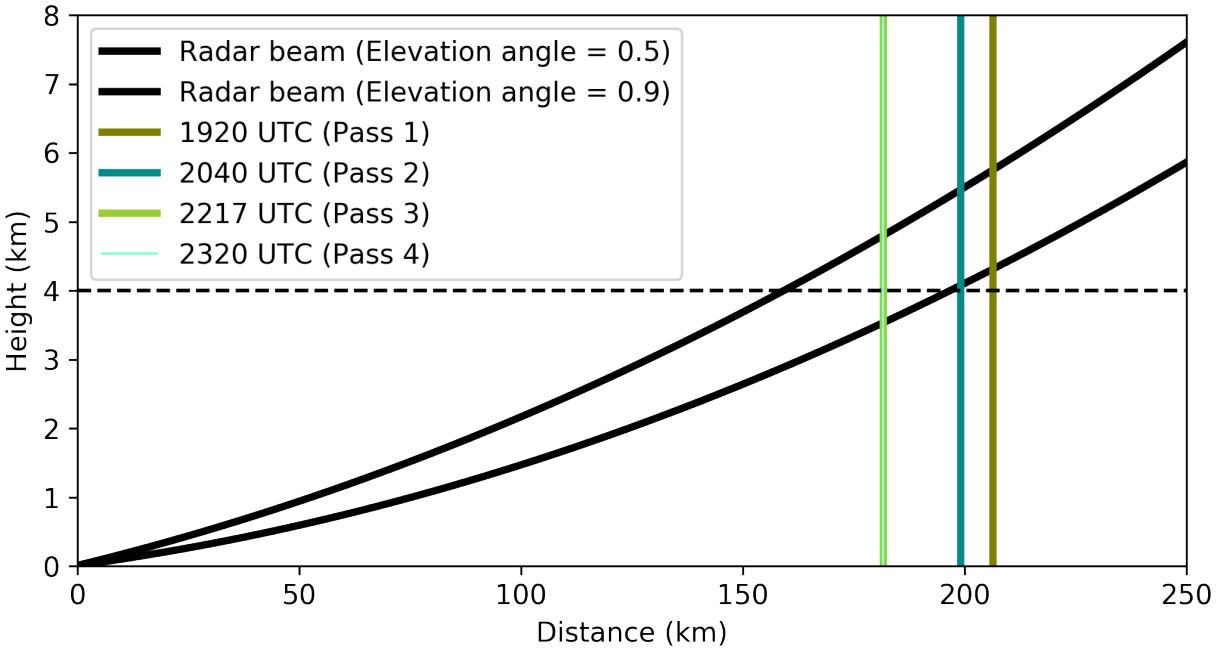

Figure 2: The radar beam height of 0.5° and 0.9° elevation angles (black solid line). The distance between the KAMX radar and the TC center of the four radar volumes corresponding to the four flight passes are highlighted by the colored vertical lines. The dashed black line represents the altitude of 4 km.

the dynamic centers is sometimes quite variable, so we would want to provide the GVTD-simplex centers as another option to derive the TC centers with high temporal resolution in this manuscript.

Discussion regarding Figure 4 on page 9: I would say the results are mixed on the improvement of the "optimal solution" over the "original solution". For example, in one pass the green dashed line looks better than the blue dashed line, but in another pass, it looks worse and in the other passes the differences are negligible. Similar things for the orange and red lines.

Thank you for the comment. Since the four solutions are quite similar with only a few m/s apart, we have calculated the RMS difference results quantitatively in Table 3 to quantitatively demonstrate that the "optimal solution" outperforms other methods, and the RMS difference of the improved GVTD solution (red) is smaller than the original GVTD solution (orange). However, similar to the response to the major comment above, we have changed the tone in the manuscript to not overly state the results.

Also, on page 9: what are the heights of comparison between the TDR and the 88D? Since the storm core is on the far edge of the 88D coverage, the beam heights are probably fairly high, and the vertical velocities could be significant in this region.

Thank you for the comment. The altitude of the analyses are added in the manuscript.

The subsequent analyses use the observations at the altitude of 4 km, so the ground-based 0.5° radar elevation beam can detect the TC inner core.

What is the impact of significant vertical velocity in the hurricane core on the TDR and 88D comparisons, given that the 88D retrievals don't take this into account?

Eq. (2) in Lee et al. 1999 shows the vertical velocity and terminal velocity term ((w-v_t)sin(ϕ)) in the construction of the Doppler velocity. They removed the contribution from w and v_t, and divided cos(ϕ) to get Eq. (3). Therefore, the vertical velocity and terminal velocity contribution becomes (w-v_t)sin(ϕ)/cos(ϕ).
sin(ϕ)/cos(ϕ) is approximate to 0 if we use the data mainly derived from the lowest scan (ϕ=0.5, sin(ϕ)/cos($\phi = 8.72 \times 10^{-3}$, Fig. 2). Therefore, the vertical velocity and terminal velocity contribution can be neglected in this case. We have added the discussion to the manuscript:

Note that $\hat{V_d}$ neglects the contribution from the terminal velocity (v_t) and vertical velocity (w) (Eq. 2 in [Lee et al., 1999]). The contribution from w and v_t is small if the elevation angle of the radar beam is low (<1°).

Lines 265 – 268, These improvements are quite small, and I am wondering if they are statistically significant? I think the authors are overstating the impact of the improvements to the GVTD technique here and some rewording is needed.

Thank you for the comment. A nonparametric Wilcoxon signed-rank test has now been conducted to test the null hypothesis that two paired sets of the RMS differences derived from the original and improved GVTD algorithms are drawn from the same distribution. Results show that the RMS difference between the original and improved GVTD algorithm is statistically significant in both single and dual-Doppler analyses with 99% confidence.

A nonparametric Wilcoxon signed-rank test is conducted to test the null hypothesis that two paired sets of the RMS differences derived from the original and improved GVTD algorithms are drawn from the same distribution. The RMS difference between the original and improved GVTD algorithms is statistically significant with a p value < 0.001 using both the projected dual-Doppler winds and single-Doppler velocities, indicating that we can reject the null hypothesis at the 1% significance level (99% confidence). The statistics suggest that the RMS differences distribution of wavenumber 0 tangential wind retrieved from the original GVTD algorithm are likely to be larger than those from the improved GVTD method.

Discussion around lines 295 – 296: these comparisons have significant differences between Ao and A1 coefficients in the eyewall region and it is not fair to say that they are "roughly consistent". Deviations of 2 m/s or less are a major error for Ao and A1 coefficients that have small values.

Thank you for the comment. We have revised the sentence.

The deviations of A_0, A_1 and B_1 coefficients between the two analyses within the eyewall

region (15 - 25 km) are less than 2 m s^{-1}.

Lines 303 – 308, please see major comment (1).

Thank you for the comment. Please refer to the response to major comment (1).

Table 3, The differences between the original and improved GVTD method are only 0.35 m/s and this difference is likely not statistically significant. See major comment (2).

Thank you for the comment. Please refer to the response to major comment (2) and comment "Lines 265 – 268", where we have changed the tone of the manuscript and conducted a statistical significane test.

Table 4, I don't understand the wavenumber magnitudes listed here. Why is the magnitude of WV0 so low? This should be azimuthal mean, correct? There is some confusion in the naming conventions listed in the table and the text that needs fixing.

Thank you for the comment. We have corrected the table caption to be more specific.

V_dD/R_T harmonics coefficients amplitude (harmonics 0 to 3) retrieved from the single Doppler and dual Doppler analyses.

Figure 6, should label these figures with the corresponding physical wind components because it is hard to follow.

Thank you for the comment. The physical wind components are added.

(a) A_0 (to obtain V_RC_0 and $V_Mcos(\theta_T - \theta_M)$) (b) A_1 (to obtain V_RC_0) (c) B_1 (to obtain V_TC_0) (d) A_2 (to obtain V_RC_0 and V_TS_1) (e) B_2 (to obtain V_TC_1) (f) A_3 (to obtain V_RC_0 and V_TS_2) (g) B_3 (to obtain V_TC_0 and V_TC_2)

References

[Bell et al., 2012] Bell, M. M., Montgomery, M. T., and Lee, W.-C. (2012). An axisymmetric view of concentric eyewall evolution in Hurricane Rita (2005). *J. Atmos. Sci.*, 69(8):2414–2432.

[Crum et al., 1998] Crum, T. D., Saffle, R. E., and Wilson, J. W. (1998). An update on the nexrad program and future wsr-88d support to operations. *Wea. Forecasting*, 13(2):253 – 262.

[Hildebrand and Mueller, 1985] Hildebrand, P. H. and Mueller, C. K. (1985). Evaluation of meteorological airborne Doppler radar. Part I: Dual-Doppler analyses of air motions. *J. Atmos. Oceanic Technol.*, 2(3):362 – 380.

[Hildebrand et al., 1994] Hildebrand, P. H., Walther, C. A., Frush, C. L., Testud, J., and Baudin, F. (1994). The ELDORA/ASTRAIA airborne Doppler weather radar: goals, design, and first field tests. *Proceedings of the IEEE*, 82(12):1873–1890.

[Jorgensen et al., 1983] Jorgensen, D. P., Hildebrand, P. H., and Frush, C. L. (1983). Feasibility test of an airborne Pulse-Doppler meteorological radar. *J. Appl. Meteor. Climatol.*, 22(5):744 – 757.

[Jou et al., 1996] Jou, B. J.-D., Deng, S.-M., and Chang, B. (1996). Determination of typhoon center and radius of maximum wind by using Doppler radar. *Atmos. Sci*, 24:1–24.

[Jou et al., 2008] Jou, B. J.-D., Lee, W.-C., Liu, S.-P., and Kao, Y.-C. (2008). Generalized VTD retrieval of atmospheric vortex kinematic structure. Part I: Formulation and error analysis. *Mon. Wea. Rev.*, 136(3):995–1012.

[Koch et al., 1983] Koch, S. E., desJardins, M., and Kocin, P. J. (1983). An interactive Barnes objective map analysis scheme for use with satellite and conventional data. *J. Appl. Meteor. Climatol.*, 22(9):1487 – 1503.

[Lee et al., 1999] Lee, W.-C., Jou, B. J.-D., Chang, P.-L., and Deng, S.-M. (1999). Tropical cyclone kinematic structure retrieved from single-Doppler radar observations. Part I: Interpretation of Doppler velocity patterns and the GBVTD technique. *Mon. Wea. Rev.*, 127(10):2419–2439.

[Lee et al., 1994] Lee, W.-C., Marks, F. D., and Carbone, R. E. (1994). Velocity track display—A technique to extract real-time tropical cyclone circulations using a single airborne Doppler radar. *J. Atmos. Oceanic Technol.*, 11(2):337–356.

[Marks et al., 1992] Marks, F. D., Houze, R. A., and Gamache, J. F. (1992). Dual-aircraft investigation of the inner core of Hurricane Norbert. Part I: Kinematic structure. *J. Atmos. Sci.*, 49(11):919–942.

[Ray and Stephenson, 1990] Ray, P. S. and Stephenson, M. (1990). Assessment of the geometric and temporal errors associated with airborne Doppler radar measurements of a convective storm. *J. Atmos. Oceanic Technol.*, 7(2):206 – 217.

[Reasor et al., 2000] Reasor, P. D., Montgomery, M. T., Marks, F. D., and Gamache, J. F. (2000). Low-wavenumber structure and evolution of the hurricane inner core observed by airborne dual-Doppler radar. *Mon. Wea. Rev.*, 128(6):1653–1680.

amt-2020-240

Thank you for reviewing the manuscript and providing constructive comments. We have made edits to the manuscript incorporated with your suggestions. Reviewers' comments are shown in black, our response to each comment is shown in blue, and changes to the manuscript are shown in red.

Reviewer #2:
Recommendation: I only found one thing to change, in the Introduction, noted below. Otherwise this a fine original paper which is perfectly suitable for publication in AMT. My comments below are mainly for the authors as I have no minor or major revisions to ask for.

Abstract: The abstract is a clear and concise description of the paper. Fine as is.

Thank you for the comment.

1. Introduction: You write " One limitation is that a ground-based Doppler radar has to be located outside of the radial distance between the radar and the storm center in order to sample the full tangential component of the vortex circulation accurately." I think you meant to write that the radar has to be outside the radius of maximum wind.It is impossible for the radar to be located farther away than the storm center to radar distance!

Thank you for the comment. We have revised the sentence.

One limitation is that the radial distance between the radar and the storm center has to be large enough to sample the tangential component of the vortex circulation in order to minimize the geometric distortion.

2. Data Sets and Methodology: This section nicely summarizes the data procedures. I am curious why the SAMURAI analyses were interpolated to a polar array while the VoRTRAC were apparently still in Cartesian form. If in fact the end result of the Vortrac analyses also ended up in polar form that should be stated here.

Thank you for the comment. We have added a comment to the manuscript to clarify.

The gridded data was further analyzed using the Vortex Objective Radar Tracking and Circulation (VORTRAC) software in LROSE to interpolate onto a cylindrical coordinate and obtain the kinematic structure by the improved GVTD algorithm formulated in section 3.1.

3. The GVTD technique improvement: 3.1: a lot of math shown here but all of it necessary. I wonder if there was earlier work on data gaps and noise influence on maximum wavenumber to retrieve. Probably not needed but I believe the code in GBVTD to select max wavenumber was developed originally by the late Tom Matejka for the Extended VAD which is an ancestor of the VTD. Well, probably too much detail for this paper anyway.

Thank you for the comment. We have added the reference of Matejka and Srivastava 1991.

To deal with missing data in observational radar data and reduce the influence of outliers [Matejka and Srivastava, 1991], the truncation of the Fourier series follows Lee et al. (2000) (Table 2), which is consistent with the restriction of maximum allowable gap size in Lorsolo and Aksoy (2012) .

3.2 GVTD-simplex center finding The description of the simplex minimization algorithm is a bit sparse. Maybe you should add a direct reference. Either that or remove the references to "contraction or expansion of the simplex" since you did not really explain what those terms mean. Also in the text when you mention comparisons of simplex-derived centers from different WSR88D radars you might list the locations: KMLB (Melbourne,FL) and KJAX (Jacksonville, FL). I think Harasti et al.(year?) had a nice description of many different of finding circulation centers.

Thank you for the comment. We have added the reference of Harasti et al. 2004 .

The simplex center is found by maximizing the mean tangential wind within an axisymmetric TC with three operations on a simplex: reflection, contraction, and expansion [Lee and Marks, 2000; Harasti et al., 2004].

Also you might mention that the "dynamic"centers are smooth because the spline fit is to only a few aircraft derived centers, One per pass, so one would not expect them to show as much variation as the G*VTD centers available every 5-6 minutes. also you have an independent wind field from SAMURAI TDR analyses.

Thank you for the comment. We have clarified the sentence.

The centers are interpolated from a few dynamic centers with a series of spline curves every two minutes, so the centers are connected into a continuous track.

Did you try simplex center finding on the pseudo-dual Doppler arrays? The Marks used the simplex to show variation of center with height in his airborne radar work and this was then later applied by Lee and Marks to the GBVTD.

Thank you for the comment. We have tried the simplex center finding on the pseudo-dual Doppler analysis, and the discrepancies between the simplex centers and dynamic centers are small. The retrieved wind fields are similar, as well as the asymmetric structure. Therefore, we decide to use the dynamic centers to be consistent with our future work discussing Hurricane Matthew's asymmetric structure observed by the ground-based radars.

4 Wind retrievals comparison between single Doppler and airborne dual Doppler analyses: This is the real meat of this paper and it is amazing that no one did this before. Maybe it had to wait for the development of GEVTD and SAMURAI before such a study could be done, but I think this part alone should be part of any class on radar meteorology from now on.

Thank you very much for the positive endorsement!

4.1 Wavenumber 0 tangential wind retrieval this section shows that GEVTD (both versions) capture well the wave 0 tangential wind by comparing with the pseudo dual Doppler analysis from the P3. This is a slick idea to generate 88d obs by projecting the TDR analysis on the 88d radials and then doing the VTD on those "data" rather than on the original 88d data. As I read this, I couldn't help thinking you could just as easily plopped some idealized vortex on Matthews position and used totally synthetic data to test the VTD algorithm performance. I am not suggesting you do this as you already have the SAMURAI analysis, just a thought that you did not need a "real" storm to do this part of the analysis.

Thank you for the comment. In response to this and another reviewer's comment, we have done an idealized experiment to show that the steady-state assumption of one straight flight leg to synthesize the data into one snapshot with the presence of rapidly evolving features could result in temporal aliasing and unrealistic asymmetric component retrievals. We have added a new subsection 4.3 and Figure 8 (Fig. 1 here) in the revised manuscript.

4.2 Asymmetric wind retrievals This is a very interesting discussion. I do wonder if the authors could say a bit more about the signature of the VRW in the reflectivity or is the VRW only visible in the wind field? It is easy to visualize in my mind the wave 1 asymmetry, but higher wave numbers make me think there should be a series of bumps in the dBZ, or is the reality that the asymmetries are more finer in scale, so requiring higher wave numbers? That is, are convective cells in the RMW giving rise to wind asymmetries that are then aliased onto wave 2? well, probably can't answer that with this dataset.

Thank you for the comment. Cha et al. 2020 shows the signature of the VRW in the reflectivity and the GVTD-retrieved tangential wind fields. The propagation speeds of asymmetric tangential wind and reflectivity signals are consistent with the linear wave theory, suggesting that the observed asymmetries are well described by VRW theory (Fig. 4 in Cha et al. 2020).
Figure 2 shows the azimuthal temporal evolution of wavenumber 1 and 2 of reflectivity and tangential wind in the inner eyewall region of Hurricane Matthew. The wavenumber 1 reflectivity is stationary from 1915 to 1945 UTC, whereas the wavenumber 2 reflectivity signals are also propagating, similar to the wavenumber 2 tangential wind signals. We have added the features description of the wavenumber 1 and 2 reflectivity signals in the manuscript, but the plot of reflectivity is not shown.

To test the hypothesis, the phases of maximum wavenumber 1 and wavenumber 2 tangential winds retrieved from the 5-minute single Doppler observations are examined in Fig. 7 for the temporal evolution during the first flight pass from 1907 to 1940 UTC. The amplitude and phase (Eqs. 18 and 19) of wavenumber 1 and 2 tangential winds are denoted in polar coordinates by the radius and azimuth, respectively. The wavenumber 1 tangential wind (Fig. 7a) generally stayed unchanged throughout the first pass with a magnitude between 8 and 12 m s^{-1} and phase to the E to NE (same as the wavenumber 1 reflectivity, not shown here). Environmental vertical wind shear derived from the Statistical Hurricane Intensity Prediction Scheme dataset (SHIPS) points to the northeast direction with a magnitude of 7 m s^{-1}, suggesting that the wavenumber 1 distribution is forced by the vertical wind shear to be consistently in the downshear-right quadrant.
The wavenumber 2 tangential wind (Fig. 7b) propagated cyclonically during the flight pass (same as the wavenumber 2 reflectivity, not shown here) with a magnitude up to 7 m s^{-1}. The propagation of the wavenumber 2 tangential wind is estimated to be 285

degrees from 1907 to 1940 UTC, which is 35 m s^{-1}, or 63% of V_{Tmax}. The propagation of the wavenumber 2 tangential wind is roughly consistent with linear VRW theory [Kuo et al., 1999], [Cha et al., 2020].

I know that VORTRAC also can produce a MSLP estimate from the symmetric wind field. I wonder if the VTD analyses give mslp similar to the flight level data. If the wind fields agree so well I would think the pressure retrievals should also. Not necessary for this paper though.

Thank you for the comment. We have computed the perturbation pressure deficit using the gradient wind balance equation. The integrated perturbation pressure deficit retrievals from different methods agree well with the 'truth'. The analysis and RMS difference of the integrated perturbation pressure deficit are added to Table 4 in the manuscript.

The perturbation pressure deficit is integrated from r = 10 to 70 km using the gradient wind balance equation [Lee et al., 2000]. The integrated perturbation pressure deficit retrievals from different methods agree well with the "truth" ($\sim$ 1 mb RMS in general). Similar as the results of RMS difference of $V_T C_0$, including the storm motion terms decreases the RMS differences about 0.2 mb. The RMS difference of improved GVTD algorithm from the single Doppler retrieval has the least deviation from the "truth", suggesting that the perturbation pressure deficit derived from the single Doppler observations has high fidelity.

5 Conclusions the authors nicely summarize their work here and hint that there is more to be said about the analyses themselves. In this paper they have validated both methods of analysis and I imagine the next Cha et al. will go into more detail about the VRW's and other features of this dataset including the eyewall replacement. This methods-oriented paper is a fine introduction to that topic.

Thank you for the comment. Some additional analyses using the improved formulation can be found in Cha (2018), with continued analysis submitted to the peer-reviewed literature in the future.

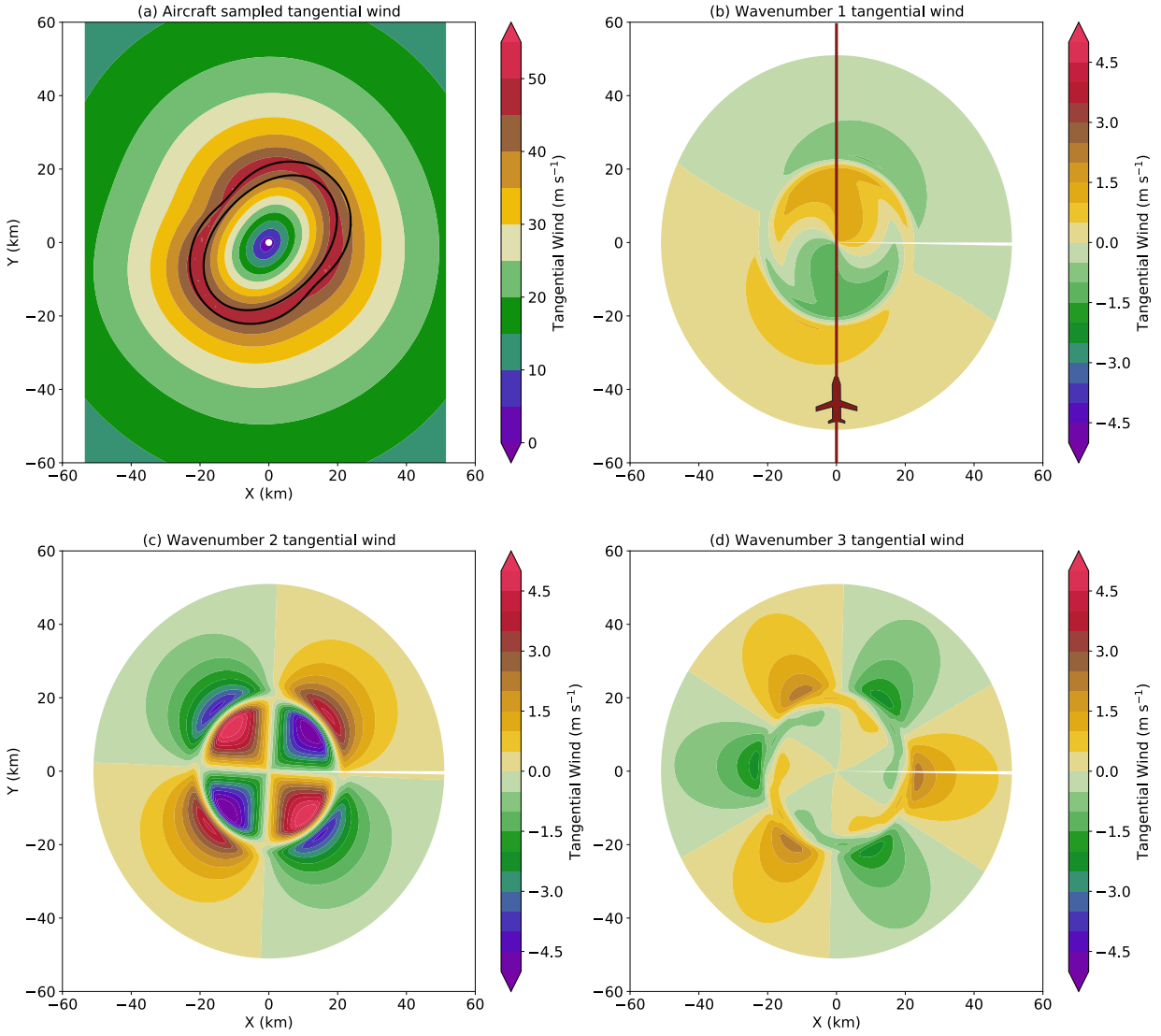

Figure 1: (a) Idealized dual-Doppler tangential wind speed retrieved from a straight flight pass through propagating wavenumber two asymmetry (color in m s^{-1}) and 50 m s^{-1} contour of time-averaged wavenumber two in black. The initial phase of the propagating wavenumber 2 tangential wind is oriented from east to west and final phase is from north to south. (b) Wavenumber 1 plus aircraft flight track from south to north, (c) Wavenumber 2, and (d) Wavenumber 3 tangential wind components retrieved by the Fourier decomposition of the tangential wind field shown in panel (a).

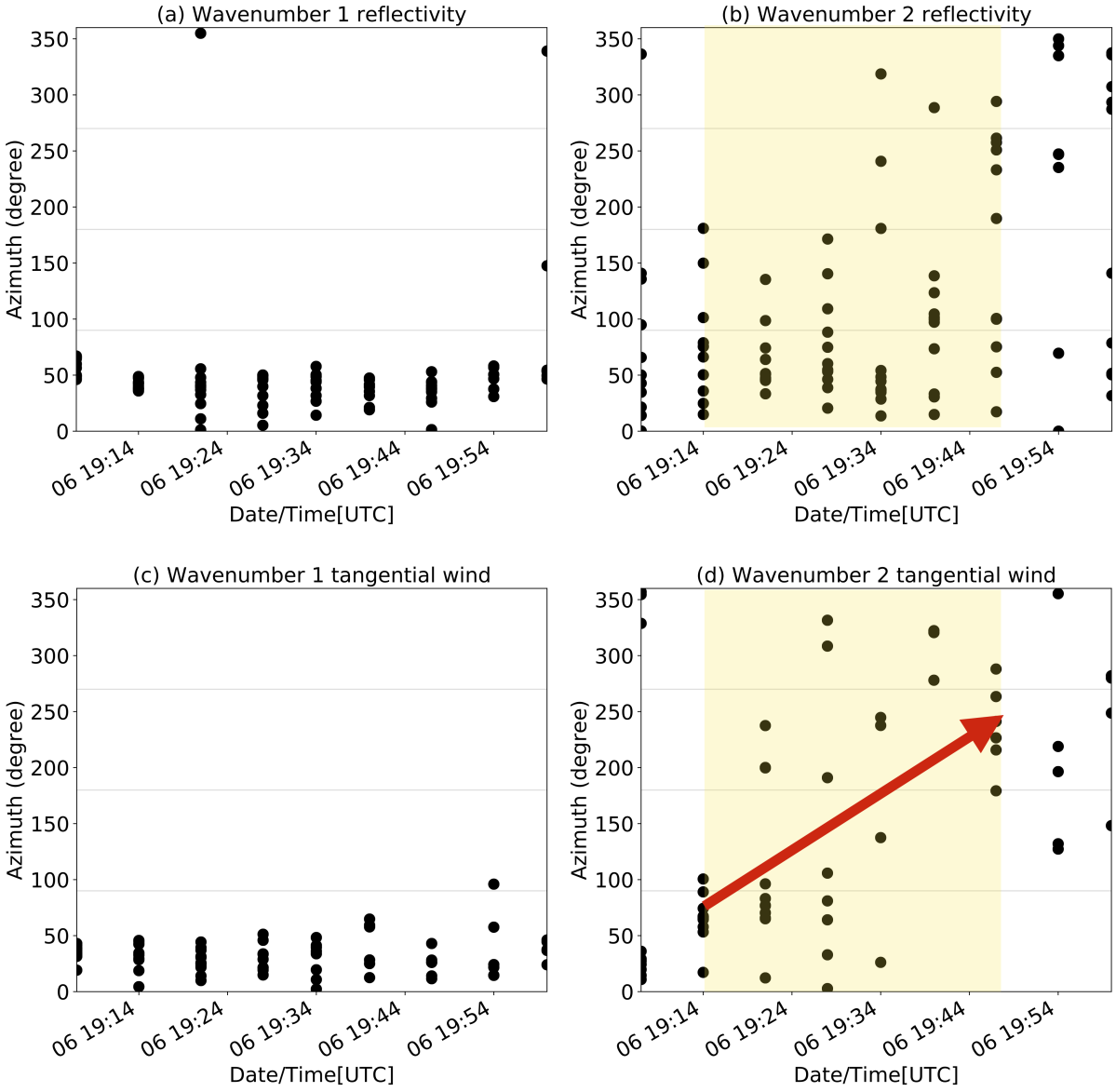

Figure 2: The azimuthal temporal evolution of wavenumber 1 and 2 of reflectivity and tangential wind in the inner eyewall region (from the radius of 15-25 km) from 1900 to 2000 UTC 6 October. The black dots are (a) Wavenumber 1 reflectivity, (b) Wavenumber 2 reflectivity, (c) Wavenumber 1 tangential wind, and (d) Wavenumber 2 tangential wind within the area from the radius of 15 to 25 km. The red arrow denotes the propagation of the median of wavenumber 2 tangential wind from 1915 to 1945 UTC, and the yellow shading illustrates the period of 1915 UTC to 1945 UTC. Adapted from Cha 2018.

References

[Cha, 2018] Cha, T.-Y. (2018). Eyewall replacement cycle of Hurricane Matthew (2016) observed by Doppler radars. *M. S. Thesis*, page Colorado State University.

[Cha et al., 2020] Cha, T.-Y., Bell, M. M., Lee, W.-C., and DesRosiers, A. J. (2020). Polygonal eyewall asymmetries during the rapid intensification of Hurricane Michael (2018). *Geophys. Res. Lett.*, 47(15):e2020GL087919.

[Harasti et al., 2004] Harasti, P. R., McAdie, C. J., Dodge, P. P., Lee, W.-C., Tuttle, J., Murillo, S. T., and Marks, F. D. (2004). Real-time implementation of Single-Doppler radar analysis methods for tropical cyclones: Algorithm improvements and use with WSR-88D display data. *Wea. Forecasting*, 19(2):219 – 239.

[Kuo et al., 1999] Kuo, H.-C., Williams, R., and Chen, J.-H. (1999). A possible mechanism for the eye rotation of Typhoon Herb. *J. Atmos. Sci.*, 56(11):1659–1673.

[Lee et al., 2000] Lee, W.-C., Jou, B. J.-D., Chang, P.-L., and Marks, F. D. (2000). Tropical cyclone kinematic structure retrieved from single-Doppler radar observations. Part III: Evolution and structures of Typhoon Alex (1987). *Mon. Wea. Rev.*, 128(12):3982–4001.

[Lee and Marks, 2000] Lee, W.-C. and Marks, F. D. (2000). Tropical cyclone kinematic structure retrieved from single-Doppler radar observations. Part II: The GBVTD-simplex center finding algorithm. *Mon. Wea. Rev.*, 128(6):1925–1936.

[Lorsolo and Aksoy, 2012] Lorsolo, S. and Aksoy, A. (2012). Wavenumber analysis of azimuthally distributed data: Assessing maximum allowable gap size. *Mon. Wea. Rev.*, 140(6):1945–1956.

[Matejka and Srivastava, 1991] Matejka, T. and Srivastava, R. C. (1991). An improved version of the Extended Velocity-Azimuth Display analysis of Single-Doppler radar data. *J. Atmos. Oceanic Technol.*, 8(4):453 – 466.

amt-2020-240

Thank you for reviewing the manuscript and providing constructive comments again. We have made edits to the manuscript incorporated with your suggestions. Reviewers' comments are shown in black, our response to each comment is shown in blue, and changes to the manuscript are shown in red.

Reviewer #3:
Review of "Comparison of Single Doppler and Multiple DopplerWind Retrievals in Hurricane Matthew (2016)" General comments: This paper evaluates the accuracy of the generalized velocity track display (GVTD) technique by comparing the wind field obtained from the airborne tail Doppler radar (TDR) data. The evaluation of the GVTD technique in a real case has not been done so far and has been desired. Additionally, this paper re-derives the GVTD technique to obtain a more accurate wind field. Generally speaking, it is hard to compare the difference between observations from different measurements because it is necessary to consider the strengths and weaknesses of each observing capability. The authors did a great job working on this difficulty by carefully looking at the retrieved wind field. This paper is well written, and the purpose and results of this study are clear. Although I have some questions to better understand the GVTD technique, I recommend acceptance once the authors address the questions.
Recommendation: Minor revisions

Specific comments:

L180: Here, I'd like to make sure which variables can actually be retrieved from Eqs. 15-19. The sentence describes that the GVTD provides the along-beam component of the mean flow (i.e., Eq. 15), axisymmetric tangential wind (i.e., Eq. 16), axisymmetric radial wind (i.e., Eq. 17), and asymmetric tangential winds (n=1-2) (i.e., Eqs. 18 and 19). But, how can we obtain axisymmetric radial wind and the along-beam component of the mean flow? Eq. 15 includes axisymmetric radial wind on the right hand side and Eq. 17 includes the along-beam component of the mean flow on the right hand side. Rearranging Eqs. 15 and 17 is needed to obtain axisymmetric radial wind and the along-beam component of the mean flow. Here, VM|| indicates VM cos (), α indicates R/RT, and the storm motion is assumed to be zero. Eq. 15:

$$V_M\ ||= A_0 - \frac{R}{R_T}V_RC_0 + \frac{1}{2}V_TS_1 - \frac{1}{2}V_RC_1 - U_Scos\theta_T - V_Ssin\theta_T$$

$$V_RC_0 = \frac{A_0 + A_1 + A_2 + A_3 + A_4}{1 + \frac{R}{R_T}} - V_Mcos(\theta_T - \theta_M) - V_RC_1 - V_RC_2 - V_RC_3 - \frac{R}{R_T}(U_Scos\theta_T + V_Ssin\theta_T)$$

Substituting Eq. 17 into Eq. 15 yields VM|| = A0 – α × ((A0+A1+A2+A3+A4)/(1+α) – VM||) + A2 + A4 (1–α) × VM|| = A0 + A2 + A4 – α × (A0+A1+A2+A3+A4)/(1+α)
Then, VM|| = (A0+A2+A4)/(1–α) – α × (A0+A1+A2+A3+A4)/(1–α^2) Substituting VM|| into Eq. 17 yields VRC0 = (A0+A1+A2+A3+A4) *(1–α)/(1–α^2) – (A0+A2+A4)/(1–α) – α × (A0+A1+A2+A3+A4)/(1–α^2)
Then, VRC0 = – (A0+A2+A4)/(1–α) + (A0+A1+A2+A3+A4)/(1–α^2) Is this derivation wrong?

Thank you for the comment. We have derived the $V_R C_0$ term to the same formula independently, but did not include that in the original manuscript. The $V_M cos(\theta_T - \theta_M)$ term can be further derived after the computation of $V_R C_0$. We have added the equation to the manuscript.

Plugging Eq. 16 into Eq. 15 to derive Eq. 20:

$$V_R C_0 = \frac{A_0 + A_1 + A_2 + A_3 + A_4}{(1 - \frac{R^2}{{R_T}^2})} - \frac{A_0 + A_2 + A_4}{(1 - \frac{R}{R_T})}$$
$$- V_R C_2 - \frac{\frac{R}{R_T}}{1 - \frac{R}{R_T}} V_R C_4 - \frac{1}{2}(\frac{1}{1 - \frac{R}{R_T}})(V_T S_5 - V_R C_5)$$

Equations 15 - 19 correspond to equations (16)-(20) in [Jou et al., 2008] with the additional terms of storm motion on Eqs. 15 - 17. Equation 20 is an updated version of Eq. 15 to minimize the unknown terms after plugging in the $V_M cos(\theta_T - \theta_M)$.

Additionally, I wonder why the authors don't evaluate the accuracy of axisymmetric radial wind in this study. If we find that both axisymmetric tangential and radial winds can be retrieved from the GVTD technique with acceptable accuracy, then the GVTD-retrieved winds can be useful for diagnosing a possibility of changes in storm size.

Thank you for the comment. As shown in the manuscript, the retrievals of A_2, A_3 are variable due to the propagation of wavenumber 2 winds. Since the axisymmetric radial wind is influenced by the harmonic 2 and 3 components, we cannot fully validate the axisymmetric radial wind retrieval. We have added a comment to the manuscript.

Since the axisymmetric radial wind is influenced by the harmonic 2 and 3 components (Eq. 20), we cannot fully validate the axisymmetric radial wind retrieval with the current dataset. The evaluation for the accuracy of the axisymmetric radial wind retrieval is not included in this study.

L218: This is just a comment. In my experience, a method from Bell and Lee (2012) provides better centers in terms of time consistency. That being said, I understand that you use the dynamic centers.

Thank you for the comment. We have tested the objective centers using Bell and Lee 2012 method, but the results are not optimal. The simplex centers are variable, so the objective method cannot get the best fit of the centers in this case.

L225: Specify the mean wind component is an unknown variable or a given value? If it is a given value, how did the authors obtain it?

Thank you for the comment. The mean wind magnitude and direction were derived from the airborne dual Doppler analysis, following the procedure proposed by [Marks et al., 1992]. The storm-relative horizontal wind field (V_r)in a cylindrical coordinate system centered on the storm can be decomposed into:

$$V_r(r, \theta, z) = \bar{V_r}(z) + V'(r, \theta, z) \quad (1)$$

where r is radius, θ is azimuth, z is height, $\bar{V}_r(z)$ is the horizontally averaged wind vector over the radius and azimuth, and $V'(r, \theta, z)$ is the deviation from $\bar{V}_r(z)$. $\bar{V}_r(z)$ can be expressed as:

$$\bar{V}_r(z) = \frac{1}{2\pi} \int_0^{2\pi} \int_0^{r_{max}} V_r(r, \theta, z) dr d\theta \tag{2}$$

If the horizontal wind field is from a circular symmetric vortex with no steering flow, $\bar{V}_r(z)$ would be zero. Nevertheless, if the vortex is embedded in the steering flow, the averaged horizontal wind field would equal the mean wind component. Thus, the local wind shear can be approximated by subtraction of the mean wind component at different altitudes. In our study, we calculated the mean wind component averaged from the vortex inner core area within the radius of 60 km. We have clarified how we derived the mean wind component in the manuscript.

The mean wind (V_M) is the horizontal average of the environmental flow at each altitude following the procedure proposed by [Marks et al., 1992], which can be used to calculate the vertical wind shear.

Figs. 3a and b: KAMX is not located at the center of the figure.
Figs. 3c and d: There is no caption about these figures.

Thank you for the comment. We have revised the caption.

Doppler velocity at z = 4 km (a) observed by KAMX radar at 1921 UTC, and (b) resampled from dual Doppler analysis synthesized from 1855 - 1940 UTC. Reflectivity at z = 4 km (c) observed by KAMX radar and (d) derived from dual Doppler analysis. The timing of (c) and (d) are the same as (a) and (b), respectively. The black star denotes the TC center, and the dashed circle denotes the radius of maximum wind of 18 km.

L303: This description appears to me that the problem comes from the airborne "dual" Doppler analysis method, which essentially uses the fore/aft scanning technique. However, I don't think that the problem here is from the steady-state assumption in the dual Doppler analysis. As described in section 1, the forward and aft scannings are conducted within a few seconds, allowing for a nearly simultaneous observation, at least, near the aircraft (thus, the steady-state assumption is valid). I thought the problem here is that retrieved wind vectors observed at different times within 45 min are synthesized into one picture in SAMURAI software, assuming that they are steady-state (e.g., Fig. 3b). Is my understanding wrong?

Thank you for the comment. This is an excellent point. We have now clarified that there are in effect two different types of sampling errors that arise from the steady state assumption – the first is due to the time lag between fore and aft beams, and the second is due to the length of time used to composite the multi-Doppler into a single snapshot. While both produce some errors, the latter is more consequential when considering low-wavenumber asymmetries since it takes longer to capture the larger scale structure, resulting in evolution over the flight pass. The 'local' wind may be correct, but the overall structure is distorted by collapsing to a single time. We hypothesize that the discrepancies of retrieved wavenumber 1 and 2 tangential winds are due to the steady state assumption in the dual Doppler wind synthesis into one snapshot, not the fore/aft lag.

We hypothesize that the discrepancies of retrieved wavenumber 1 and 2 tangential winds are due to the steady state assumption in the dual Doppler wind synthesis into one snapshot. Two different types of sampling errors in effect arise from the steady state assumption – the first is due to the time lag between fore and aft beams, and the second is due to the length of time used to composite the multi-Doppler into a single snapshot. While both produce some errors, the latter is more consequential when considering the temporal evolution of the phenomena is faster than the period of data collection, resulting in evolution over the flight pass. The "local" wind may be correct, but the overall structure is distorted by collapsing to a single time. For example, the propagation velocity of a wavenumber 2 vortex Rossby wave (VRW) is half of the symmetric tangential wind velocity [Lamb, 1932, Guinn and Schubert, 1993, Kuo et al., 1999]. A propagating wavenumber 2 asymmetry could then alias onto other wavenumbers, contributing to a discrepancy in wavenumber 1 tangential wind.

References

[Bell and Lee, 2012] Bell, M. M. and Lee, W.-C. (2012). Objective tropical cyclone center tracking using single-Doppler radar. *Journal of Applied Meteorology and Climatology*, 51(5):878–896.

[Guinn and Schubert, 1993] Guinn, T. A. and Schubert, W. H. (1993). Hurricane spiral bands. *Journal of the Atmospheric Sciences*, 50(20):3380–3403.

[Jou et al., 2008] Jou, B. J.-D., Lee, W.-C., Liu, S.-P., and Kao, Y.-C. (2008). Generalized VTD retrieval of atmospheric vortex kinematic structure. Part I: Formulation and error analysis. *Mon. Wea. Rev.*, 136(3):995–1012.

[Kuo et al., 1999] Kuo, H.-C., Williams, R., and Chen, J.-H. (1999). A possible mechanism for the eye rotation of Typhoon Herb. *J. Atmos. Sci.*, 56(11):1659–1673.

[Lamb, 1932] Lamb, H. (1932). *Hydrodynamics*. Cambridge university press.

[Marks et al., 1992] Marks, F. D., Houze, R. A., and Gamache, J. F. (1992). Dual-aircraft investigation of the inner core of Hurricane Norbert. Part I: Kinematic structure. *J. Atmos. Sci.*, 49(11):919–942.

Comparison of Single Doppler and Multiple Doppler Wind Retrievals in Hurricane Matthew (2016)

Ting-Yu Cha[1] and Michael M. Bell[1]

[1]Department of Atmospheric Science, Colorado State University, Fort Collins, Colorado, United States

Correspondence: Ting-Yu Cha (tingyu@colostate.edu)

Abstract. Hurricane Matthew (2016) was observed by the ground-based polarimetric Next Generation Weather Radar (NEXRAD) in Miami (KAMX) and NOAA P-3 airborne tail Doppler radar near the coast of the southeastern United States for several hours, providing a novel opportunity to evaluate and compare single and multiple Doppler wind retrieval techniques for tropical cyclone flows. The generalized velocity track display (GVTD) technique can retrieve a subset of the wind field from a single ground-based Doppler radar under the assumption of nearly axisymmetric rotational wind, but is shown to have errors from aliasing of unresolved wind components. An improved technique that mitigates errors due to storm motion is derived in this study, although some spatial aliasing remains due to limited information content from the single Doppler measurements. A spline-based variational wind retrieval technique called SAMURAI can retrieve the full three-dimensional wind field from airborne radar fore-aft pseudo-dual Doppler scanning, but is shown to have errors due to temporal aliasing from the non-simultaneous Doppler measurements. A comparison between the two techniques shows that the axisymmetric tangential winds are generally comparable between the two techniques~~after the improvements to GVTD retrievals~~, and the improved GVTD technique improves the accuracy of the retrieval. Fourier decomposition of asymmetric kinematic and convective structure shows more discrepancies due to spatial and temporal aliasing in the retrievals. The strengths and weaknesses of each technique for studying tropical cyclone structure are discussed, and suggest that complementary information can be retrieved from both single and dual Doppler retrievals. Future improvements to the asymmetric flow assumptions in single Doppler analysis and steady-state assumptions in pseudo-dual Doppler analysis are required to reconcile differences in retrieved tropical cyclone structure.

1 Introduction

Doppler radar can provide high-resolution wind measurements within tropical cyclones (TCs), but the measurement is limited to the projection of the wind along the radial direction of the radar beam. Wind retrieval techniques are therefore required in order to identify the convective and kinematic structure of TCs from either single or multiple Doppler observations. While multiple Doppler retrievals are generally superior for deriving three-dimensional winds, measurements from two or more radars are not generally available and are often not simultaneous. In addition to the presence of ~~two or more~~ an airborne Doppler radar with fore/aft capability or multiple radars with sufficient range and geometry around the TC, a steady state assumption during the Doppler radar observation period is required to synthesize the wind fields into one snapshot in time. The steady state as-

sumption is less severe for single Doppler wind retrievals, but more assumptions about the unresolved components of the flow are required. ~~The strengths and weaknesses of different platform observing capabilities and retrieval techniques for~~ Previous studies have shown the intercomparison of dual Doppler wind fields from two orthogonal flight legs and a ground-based two-radar network (Jorgensen et al., 1983; Hildebrand and Mueller, 1985). Several other studies have investigated both single and multi-Doppler techniques for retrieving TC wind fields (Lee et al., 1994; Crum et al., 1998; Reasor et al., 2000; Lee et al., 1999; Jou et but the strengths and weaknesses of different techniques have not been compared and addressed fully. In this study, ground-based single Doppler and airborne dual Doppler observations simultaneously sampling Hurricane Matthew (2016) are analyzed to provide the first comprehensive comparison between ~~the two~~ ground-based single and airborne multi-Doppler wind retrieval techniques in a TC.

One of the primary dual-Doppler platforms for TC studies is the airborne National Oceanic and Atmospheric Administration WP-3D (NOAA P-3) tail Doppler radar (TDR), which can obtain kinematic structure for storms well away from the U.S. coast. The TDR has been used since the early 1980's for airborne radar data collection in hurricane reconnaissance and research missions. In early usage, the wind field was reconstructed from using pseudo-dual Doppler analysis of two flight legs that were perpendicular to each other known as the "L" pattern (Marks and Houze, 1984, 1987). The "L" pattern takes a period of 0.5 to 1 hour to complete, such that some slowly evolving wind asymmetries can be deduced (Marks et al., 1992), but more rapidly evolving structure cannot be retrieved by this technique.

In Lee et al. (1994), the Velocity Track Display (VTD) technique was proposed to retrieve the TC kinematic structure from a single airborne Doppler radar. The VTD technique takes advantage of the Doppler signatures of a vortex with a dipole pattern of approaching and receding velocities. The linear least squares method is utilized to fit Fourier basis functions onto the Doppler velocity, such that a subset of the wind field can be retrieved for each radius and altitude based on the Fourier coefficients. VTD retrievals from Hurricane Gloria (1985) were compared with pseudo-dual Doppler analysis constructed from two orthogonal flight legs under the assumption that the circulation was in a steady state over 1-2 hour period. Lee et al. (1994) concluded that spatial and temporal aliasing in the pseudo-dual Doppler analysis over long periods tended to create artificial higher wavenumbers and reduce the wind maxima compared to the single Doppler retrievals. The study was one of the first to quantify the accuracy of low-wavenumber TC asymmetries from multiple Doppler analysis due to the evolving weather.

The "Fore/Aft Scanning Technique" (FAST) was proposed by Hildebrand et al. (1986) in which the antenna alternately scans forward and then aft of the flight track within a few seconds, which could produce more accurate local wind estimations. This scanning methodology can gather data faster, mitigating some of the impact from weather evolution, and no longer requires the execution an "L" shaped flight pattern (Gamache et al., 1995). The FAST approach produces horizontal winds with high accuracy, and can yield vertical motion through the mass continuity equation or a multi-beam technique with multiple aircraft (Jorgensen et al., 1996). The FAST scanning strategy has been used almost exclusively in recent years, and has provided significant advances of our understanding of TC structure and dynamics (Lee et al., 2003; Houze, 2010).

Although dual-Doppler observations can be used to assess snapshots of high resolution kinematic and convective structure, airborne reconnaissance and research missions are rare events in most of the countries impacted by TCs. The three-dimensional

airflow structure can also be retrieved from the dual-Doppler observations when the system is detected by two ground-based radars. ~~Such dual-Doppler radar observations~~ General sources of error in the inter-comparison of ground-based and airborne dual-Doppler observations include instrument effects, algorithm effects, and sampling effects (Hildebrand and Mueller, 1985). Instrument effects include the effects of attenuation, signal-to-noise ratio, and the number of radar samples that could be caused by the radar processor design or measurement technique. These effects are likely to be most influential with marginal signal-to-noise, but random velocity errors up to 1 m s^{-1} are possible with many radar designs, including airborne radars (Hildebrand et al., 1994). Algorithm effects include the effects of the interpolation to the Cartesian grid, multi-Doppler geometry, the solution method and its associated assumptions, and the derivation of the vertical velocities. Sampling effects include the effects of data spacing and density, geometry of flight tracks, temporal changes in the storm, advection, and data collection period. One of the long-lasting problems is the length of time required for each flight leg with airborne Doppler radar (Ray and Stephenson, 1990).The temporal effects can degrade the analysis if the data collection takes too long. Jorgensen et al. (1983) quan compared the wind fields of homogeneous precipitation derived from the two pseudo-orthogonal flight legs and two ground-based dual-Doppler observations. Their measurements showed agreement in the horizontal wind fields, but small discrepancies in the vertical velocities about 0.5 - 1 m s^{-1} for the airborne system and about 0.2 m s^{-1} for the ground-based system. The discrepancy was attributed to uncertainties in the pointing angle of the airborne system and a long data collection period.

Ground-based dual-Doppler radar observations of TCs are usually limited ~~by the radar range with only a small portion of TC (Jou et al., 1996)~~ to the observation of storms that happen to develop or move within the domain covered by the radars and extensive radar baselines Jou et al. (1996). The range limitation of ground-based radar observations can restrict the operational exploitation of dual Doppler measurements ~~such that the wind retrieval based on single Doppler techniques is often required~~ due to the large spacing between coastal radars and limited dual-Doppler lobes. As such, single Doppler retrieval techniques are often required to estimate the vortex structure.

The Ground-based velocity track display (GBVTD) was developed by Lee et al. (1999) as an extension of VTD for stationary radar scanning geometry. The GBVTD technique provides a new way to examine axisymmetric and asymmetric structures of a TC near landfall from single ground-based Doppler radar, and has been successfully utilized in several studies (Lee et al., 2000; Lee and Bell, 2007; Zhao et al., 2008, 2012; Shimada et al., 2018). One limitation is that ~~a ground-based Doppler radar has to be located outside of~~ the radial distance between the radar and the storm center ~~in order to sample the full~~ has to be large enough to sample the tangential component of the vortex circulation ~~accurately~~in order to minimize the geometric distortion. Additionally, the GBVTD technique cannot fully separate the asymmetric components of the tangential and radial wind or the mean environmental wind due to spatial aliasing. Extensions to the GBVTD technique have been developed to better resolve asymmetries when multiple radars are available (EGBVTD) (Liou et al., 2006) or to resolve the mean wind when sufficient scatterers are near the radar (MGBVTD) (Chen et al., 2013).

The generalized velocity track display (GVTD) (Jou et al., 2008) is a technique that improves upon GBVTD by introducing an aspect ratio calculated by multiplying the distance of each gate (D) by measured Doppler velocity (V_d) and then scaling by the distance between the radar and the TC center (R_T). Key vortex kinematic structures displayed in the $V_d D/R_T$ space simplify the interpretation of the radar signature and eliminate the geometric distortion inherited in the V_d space (Jou et al.,

1996). GVTD expands $V_d D/R_T$ into Fourier coefficients in a linear coordinate (θ') rather than expanding V_d in a nonlinear coordinate (ψ') in GBVTD. The geometry and symbols of GVTD are displayed in Fig. 1. The retrieved wind field from GVTD is no longer limited by the analysis domain due to the required approximation of cosα in GBVTD (Eq. (5) in Lee et al. (1999)), and the retrieved asymmetric structures are without distortion. The percentage errors of the retrieved wavenumber 2 and 3 asymmetries are negligible (<1%) in general, which agrees well with the analytical solutions. Also, the GVTD formulation can be applied to the extensions of the velocity track display (VTD) techniques (e.g. GBVTD-simplex, Lee and Marks (2000)) to improve their performance. Therefore, it not only expands the capability of using ground-based Doppler radar data in TC forecasts but provides researchers an opportunity to examine TC kinematic and some derived dynamic variables in detail (such as vertical velocity, angular momentum, and vertical vorticity).

Jou et al. (2008) tested the GVTD technique with idealized vortices and confirmed that the modification by the aspect ratio is beneficial to retrieve the vortex kinematic structure. Although the GVTD technique largely improves and extends the capability of GBVTD, several limitations of the single-Doppler measurement remain. In particular, the equations are still underdetermined, and require a closure assumption in order to retrieve the asymmetric wind field.

The primary motivation of this study is to compare the strengths and weaknesses of the GVTD-technique and ~~a~~ an airborne dual-Doppler wind-synthesis analysis in a real case, which has not been done in previous studies. Hurricane Matthew (2016) was observed by the Next Generation Weather Radar (NEXRAD) radar in Miami (KAMX), concurrently with the NOAA P-3 (hereafter P3) airborne radar when it approached the southeastern United States. The KAMX radar has a larger data coverage, but the P3 has better spatial resolution due to its closer range. Since airborne and ground-based radar collected data simultaneously, the case provides a unique opportunity to evaluate the wind retrievals. The datasets and methodology are described in section 2. The improved algorithm of the GVTD is formulated in section 3. In section 4, the improved GVTD algorithm is applied to the NEXRAD data in Hurricane Matthew (2016) and compared with the retrieved winds from the dual Doppler analysis. A summary of our results and conclusions are presented in section 5.

2 Datasets and methodology

Hurricane Matthew (2016) was the first Category 5 hurricane in the Atlantic basin since 2007, and caused widespread damage across its destructive path. When Matthew moved parallel to the east coast of Florida, it was observed simultaneously by the KAMX single Doppler radar at a 5-minute interval and the P3 TDR from 19 UTC 6 October to 00 UTC 7 October with four flight passes through the center during Matthew's eyewall replacement process.

The flight track of the P3 and the detecting range of the KAMX radar are displayed in Fig. 2a. All radar sweep files were initially processed using an automated quality control (QC) script using National Center for Atmospheric Research (NCAR) SoloII software (Bell et al., 2013) and then manually edited to unfold the Doppler velocity aliasing and remove the discontinuities and noise echoes. A coordinate transform and interpolation were applied to the KAMX radar fields from the original plan position indicators (PPIs) to the constant-altitude plan position indicators (CAPPIs) in Cartesian coordinates using Radx2Grid in the Lidar Radar Open Software Environment (LROSE) software (Bell, 2019). The gridded domain is 400 km ×

400 km with a horizontal grid spacing of 1 km and vertical grid spacing of 0.5 km. While the vertical resolution may be a bit fine, we focus on the horizontal structure which is appropriately resolved for the given sampling. The gridded data was further analyzed using the Vortex Objective Radar Tracking and Circulation (VORTRAC) software in LROSE to interpolate onto a cylindrical coordinate and obtain the kinematic structure by the improved GVTD algorithm formulated in section 3.1.

The P3 was involved in the reconnaissance mission from 19 UTC 6 October to 00 UTC 7 October. The P3 was equipped with the TDR, which scanned in FAST mode in order to obtain pseudo dual-Doppler measurements. The TDR documented the intensification and weakening stages of Matthew's ERC. The P3 flew four radial passes through the center of the TC, with each pass being 30 to 60 minutes apart. The time window of the four passes are listed in Table 1, while the location of each pass is shown in Fig. 2a. The storm center and storm motion were both estimated from the Hurricane Research Division (HRD) aircraft-derived dynamic center (Willoughby and Chelmow, 1982). The analysis track for dual-Doppler analyses was linearly interpolated from each dynamic center using the derived storm motion. The dual-Doppler analysis was synthesized with each of the P3 radial passes at 1-km horizontal grid spacing and 0.5 km vertical grid spacing using SAMURAI software (Bell et al., 2012) in LROSE. The grid spacing should be smaller than the data spacing in order to accurately resolve the maximum spatial scales available for the given sampling (Koch et al., 1983). A low-pass filtering was applied to the P-3 analysis to ensure that the resolved scales were in fact consistent with the data spacing. SAMURAI is a three-dimensional variational data assimilation tool that uses a finite element basis to estimate the most likely state of the atmosphere given a set of observations. The ~~analysis~~ algorithm effects of SAMURAI have been tested in Bell et al. (2012) which the analysis has high fidelity to the observations, with linear correlations of 0.99 and linear slope and bias values near one and zero, respectively. The analysis was initially done on a Cartesian coordinate and then interpolated onto a cylindrical coordinate with azimuthal resolution of 1 degree and radial resolution of 1 km. The four passes were analyzed in detail to examine the changes in kinematic structure with high spatial resolution over four hours, with a particular focus on the first pass in this study.

3 The GVTD technique improvement

The Doppler velocity in Jou et al. (2008) is decomposed into tangential, radial, and mean wind components where storm motion is an implicit element in the mean wind component. The mean wind (V_M) is the horizontal average of the environmental flow at each altitude following the procedure proposed by Marks et al. (1992), which can be used to calculate the vertical wind shear. While the divergence of the environmental flow may not be zero since the environmental flow is not constant in the horizontal direction (Chan and Gray, 1982; Chan, 1984), we assume a horizontally homogeneous mean wind in the following derivation. This assumption is different than the original derivation in Jou et al. (2008) where the mean wind is a function of radius and height. Storm motion (U_S, V_S) is defined here as the deep layer motion vector over the whole vortex that varies only in time and does not vary with height or radius. The remaining terms in the GVTD formulation, namely the tangential (V_T)and radial (V_R) winds, are functions of radius, height and azimuth to the storm center. Despite the fact that the environmental wind is an important factor to determine storm motion, the storm motion and environmental wind are not the same component due to vertical wind shear.

The storm motion and mean wind component were originally combined together in GVTD and affected the retrievals of the mean wind, and axisymmetric (wavenumber 0) tangential and radial winds. Notably, they do not have an influence on retrieving the phase and magnitude of GVTD-asymmetric components of tangential wind. However, when the storm moves fast or there is a high deviation of direction between mean wind and storm motion they can produce errors. To resolve this error, we re-derive the GVTD technique and separate the storm motion from the mean wind component.

3.1 Mathematical formulation

Following the symbols and geometry utilized in the GBVTD (Lee et al., 1999) and GVTD (Jou et al., 2008) techniques, the addition of the storm motion to the geometry is illustrated in Fig. 1. We start with the horizontal projection of the Doppler velocity:

$$V_d\hat{V}_d/cos\phi = V_M cos(\theta_d - \theta_M) - V_T sin\psi + V_R cos\psi \tag{1}$$

where ϕ is the elevation angle of the radar, θ_d is the mathematical angle of the radar measured from the east, θ_M is the direction of mean wind, and ψ is the angle composed by the measured radar beam to the radar and the measured radar beam to the storm center. Note that $\hat{V}_d$ neglects the contribution from the terminal velocity (v_t) and vertical velocity (w) (Eq. 2 in Lee et al. (1999)). The contribution from w and v_t is small if the elevation angle of the radar beam is low ($<1°$). In this study, the storm motion (U_S, V_S) is added into the equation as an independent, known variable that projects onto the Doppler velocity, such that:

$$V_d\hat{V}_d/cos\phi = V_M cos(\theta_d - \theta_M) + U_S cos\theta_d + V_S sin\theta_d - V_T sin\psi + V_R cos\psi \tag{2}$$

where $\psi = \theta - \theta_d$. Rearranging Eq. 2, we obtain

$$\begin{aligned}\hat{V}_d/cos\phi &= V_M cos(\theta_d - \theta_M) - V_T sin(\theta - \theta_d) + V_R cos(\theta - \theta_d) + U_S cos\theta_d + V_S sin\theta_d \\ &= V_M(cos\theta_d cos\theta_M + sin\theta_d sin\theta_M) - V_T(sin\theta cos\theta_d - cos\theta sin\theta_d) \\ &+ V_R(cos\theta cos\theta_d + sin\theta sin\theta_d) + U_S cos\theta_d + V_S sin\theta_d\end{aligned} \tag{3}$$

The radar angle θ_d can be denoted as:

$$\begin{aligned}Dcos\theta_d &= Rcos\theta + R_T cos\theta_T \\ Dsin\theta_d &= Rsin\theta + R_T sin\theta_T\end{aligned} \tag{4}$$

Plugging Eq. 4 into Eq. 3 and approximating ~~$V_d/cos\phi$~~ $\hat{V}_d/cos\phi$ with V_d ~~at low elevation angles~~(only valid when the elevation angle is low):

$$V_d = (-V_T sin\theta + V_R cos\theta + V_M cos\theta_M + U_S)(Rcos\theta + R_T cos\theta_T)/D$$
$$+ (V_T cos\theta + V_R sin\theta + V_M sin\theta_M + V_S)(Rsin\theta + R_T sin\theta_T)/D \quad (5)$$

Rearranging Eq. 5 and let $\theta' = \theta - \theta_T$, we obtain:

$$\begin{aligned} V_d\frac{D}{R_T} &= [V_R\frac{R}{R_T} + V_M cos(\theta_T - \theta_M) + U_S cos\theta_T + V_S sin\theta_T] \\ &- [V_T + \frac{R}{R_T}(V_M sin(\theta_T - \theta_M) + U_S sin\theta_T - V_S cos\theta_T)]sin\theta' \\ &+ [V_R + \frac{R}{R_T}(V_M cos(\theta_T - \theta_M) + U_S cos\theta_T + V_S sin\theta_T)]cos\theta' \end{aligned} \quad (6)$$

Decomposing $V_d D/R_T$, V_T, and V_R into Fourier components in the θ' coordinates:

$$V_d\frac{D}{R_T}(R,\theta') = A_0 + \Sigma A_n cosn\theta' + \Sigma B_n sinn\theta' \quad (7)$$

$$V_T(R,\theta') = V_T C_0 + \Sigma V_T C_n cosn\theta' + \Sigma V_T S_n sinn\theta' \quad (8)$$

$$V_R(R,\theta') = V_R C_0 + \Sigma V_R C_n cosn\theta' + \Sigma V_R S_n sinn\theta' \quad (9)$$

where A_n ($V_T C_n$ and $V_R C_n$) and B_n ($V_T S_n$ and $V_R S_n$) are the amplitude of the azimuthal wavenumber n cosine and sine components, as defined in Lee et al. (1999); Jou et al. (2008). Substituting Eqs. 7, 8, and 9 into Eq. 6, we obtain the following expressions for the relation between the Fourier coeffients and wind components:

$$A_0 = \frac{R}{R_T}V_R C_0 + V_M cos(\theta_T - \theta_M) - \frac{1}{2}V_T S_1 + \frac{1}{2}V_R C_1 + U_S cos\theta_T + V_S sin\theta_T \quad (10)$$

$$A_1 = \frac{R}{R_T}V_R C_1 + \frac{R}{R_T}(V_M cos(\theta_T - \theta_M) + U_S cos\theta_T + V_S sin\theta_T) + V_R C_0 - \frac{1}{2}V_T S_2 + \frac{1}{2}V_R C_2 \quad (11)$$

$$B_1 = \frac{R}{R_T}V_R S_1 - \frac{R}{R_T}(V_M sin(\theta_T - \theta_M) + U_S sin\theta_T - V_S cos\theta_T) - V_T C_0 + \frac{1}{2}V_T C_2 + \frac{1}{2}V_R S_2 \quad (12)$$

$$A_n(n \geq 2) = \frac{R}{R_T} V_R C_n + \frac{1}{2}(V_T S_{n-1} + V_R C_{n-1} - V_T S_{n+1} + V_R C_{n+1}) \tag{13}$$

$$B_n(n \geq 2) = \frac{R}{R_T} V_R S_n + \frac{1}{2}(-V_T C_{n-1} + V_R S_{n-1} + V_T C_{n+1} + V_R S_{n+1}) \tag{14}$$

The Fourier coefficients can be rearranged to obtain each wind component of the vortex:

$$V_R C_0 = \frac{A_0 + A_1 + A_2 + A_3 + A_4}{1 + \frac{R}{R_T}} - V_M cos(\theta_T - \theta_M) - V_R C_1 - V_R C_2 - V_R C_3 - \frac{R}{R_T}(U_S cos\theta_T + V_S sin\theta_T) \tag{15}$$

$$V_M cos(\theta_T - \theta_M) = A_0 - \frac{R}{R_T} V_R C_0 + \frac{1}{2} V_T S_1 - \frac{1}{2} V_R C_1 - U_S cos\theta_T - V_S sin\theta_T \tag{16}$$

$$V_T C_0 = -B_1 - B_3 + \frac{R}{R_T}[-V_M sin(\theta_T - \theta_M) + V_R S_1 + V_R S_3 - U_S sin\theta_T + V_S cos\theta_T] + V_R S_2 \tag{17}$$

$$V_T S_n = 2A_{n+1} - V_R C_n + V_T S_{n+2} - V_R C_{n+2} - 2\frac{R}{R_T} V_R C_{n+1} \tag{18}$$

$$V_T C_n = -2B_{n+1} + V_R S_n + V_T C_{n+2} + V_R S_{n+2} + 2\frac{R}{R_T} V_R S_{n+1} \tag{19}$$

Plugging Eq. 16 into Eq. 15:

$$V_R C_0 = \frac{A_0 + A_1 + A_2 + A_3 + A_4}{(1 - \frac{R^2}{R_T{}^2})} - \frac{A_0 + A_2 + A_4}{(1 - \frac{R}{R_T})} - V_R C_2 - \frac{\frac{R}{R_T}}{1 - \frac{R}{R_T}} V_R C_4 - \frac{1}{2}(\frac{1}{1 - \frac{R}{R_T}})(V_T S_5 - V_R C_5) \tag{20}$$

Equations 15- 19 correspond to equations (16)-(20) in Jou et al. (2008) with the additional terms of storm motion on Eqs. 15 - 17. Equation 20 is an updated version of Eq. 15 to minimize the unknown terms after plugging in the $V_M cos(\theta_T - \theta_M)$. The derivation shows that the storm motion is aliased on the components of mean wind, wavenumber 0 tangential and wavenumber 0 radial wind. Since the storm motion can be accurately estimated over successive radar volumes, the above equations can yield more accurate estimation of these wind components. However, the separation of storm motion and mean wind does not solve the underdetermined problem that the number of unknown variables is greater than the number of equations. We apply the same

closure assumption in Lee et al. (1999) and Jou et al. (2008) that the asymmetric component of radial wind is much smaller than the asymmetric component of tangential wind, so the terms associated with radial wind asymmetries can be ignored. This closure assumption may not be applicable within the boundary layer or outflow layer where the radial wind asymmetries can be substantial. Future research is required to improve this closure assumption and retrieve the asymmetric radial wind.

With the above equations, the along-beam component of the mean flow, axisymmetric (n=0) tangential wind, axisymmetric radial wind, and asymmetric tangential winds (n=1-2) can be retrieved by performing linear least squares fit on $V_d D/R_T$ in a TC centered cylindrical coordinate. All data within 1-km radius-wide annulus are included in the linear least squares fit. To deal with missing data in observational radar data and reduce the influence of outliers (Matejka and Srivastava, 1991), the truncation of the Fourier series follows Lee et al. (2000) (Table 2), which is consistent with the restriction of maximum allowable gap size in Lorsolo and Aksoy (2012). Lorsolo et al. have shown that the maximum allowable gap size varies with number of gaps and noise. If more gaps are present in the signal, the maximum allowable gap size is greater than originally suggested in Lee et al. (2000). We allowed the maximum wavenumber up to wavenumber 2 in the retrieved tangential wind in this study to reduce retrieval errors.

3.2 GVTD-simplex center finding

The GVTD algorithm can be highly sensitive to the center location. Jou et al. (2008) showed that the uncertainty of the center location cannot exceed 5 km, or about 20% of the radius of the maximum wind (RMW), in order to have a reasonable wind retrieval. There are several ways to identify TC center, such as the geometric center (Griffin et al., 1992), wind center (Wood and Brown, 1992), dynamic center (Willoughby and Chelmow, 1982) and vorticity center (Marks et al., 1992). The centers identified by different methods are not necessarily collocated, and the range of uncertainties is a few kilometers or more. Since both vorticity centers estimated from the GVTD technique and dynamic centers derived from the aircraft reconnaissance were available, the comparison of the different centers is required in order to have a better result of wind retrieval.

The GBVTD-simplex algorithm is a method to identify TC vorticity centers using single-Doppler radar data developed by Lee and Marks (2000). The simplex center is found by maximizing the mean tangential wind within an axisymmetric TC with three operations on a simplex: reflection, contraction, and expansion (Lee and Marks, 2000; Harasti et al., 2004). The GBVTD-simplex algorithm reduces the uncertainties in estimating TC position and improves the quality of the GBVTD-retrieved TC circulation. The deviation of the true centers to the GBVTD-simplex center in an idealized TC is approximately 340 m. In this study, since the GVTD technique has better wind field estimation, we conducted the GVTD-simplex method to estimate the centers following the GBVTD-simplex algorithm. By maximizing GVTD-retrieved mean tangential wind, using the GVTD technique to estimate the TC vorticity center has higher accuracy than the GBVTD technique.

The GVTD-simplex method is performed as the following procedure:

(1) Doppler velocities on a CAPPI were interpolated onto a cylindrical grid with 1-km radial spacing centered at a given TC center.

(2) Find the TC center possessing the highest mean tangential wind within an axisymmetric TC.

(3) Use three operations on a simplex : reflection, contraction, and expansion - to search for a new maximum or minimum in

the field around the simplex. We put the dynamic center from HRD as the first guess. The operation process would start from this point and find the circulation center.

To compare the performance of GVTD-simplex and GBVTD-simplex centers, the dynamic centers from HRD (Willoughby and Chelmow treated as the reference center because they are consistently centered at the geometric center of the storm over our analysis period compared to the simplex centers. The ~~continuous~~ centers are interpolated from ~~the~~ a few dynamic centers with a series of spline curves every two minutes, so the centers are connected into a continuous track. Figure 2b shows that the centers retrieved by the GVTD-simplex method are not consistent with that of the retrievals from the GBVTD-simplex method, which is due to the more accurate estimation of axisymmetric tangential wind. Although the GVTD-simplex centers follow more closely to the dynamic centers over the 35 hours of observation, the location of the GVTD-simplex center is still variable, similar as GBVTD-simplex center (Lee and Marks, 2000) and not fully consistent with different radar retrievals (such as KAMX vs. KMLB, and KMLB vs. KJAX). Since the ~~GVTD technique is highly sensitive to the storm center and the~~ dynamic centers are qualitatively and quantitatively better than the simplex centers in terms of consistency, and are independent of assumptions in either the airborne dual-Doppler and single-Doppler retrievals, our study utilized the dynamic centers to perform the GVTD technique and cylindrical decomposition of the airborne wind field.

4 Wind retrievals comparison between single Doppler and airborne dual Doppler analyses

4.1 Wavenumber 0 tangential wind retrieval

The dual Doppler analyses from the four aircraft passes into Hurricane Matthew are optimal to evaluate the performance of the GVTD technique because we can obtain all coefficients (Eqs. ~~15 to 19~~16 to 20) from the Fourier decomposition of V_T and V_R, known storm motion, and mean wind components, which ensures the comparability of the wind field. To evaluate the improved algorithm, the wind fields from the dual Doppler analyses were resampled into Doppler velocity that would be observed by the KAMX radar. The subsequent analyses use the observations at the altitude of 4 km, so the ground-based 0.5° radar elevation beam can detect the TC inner core. The wind fields were then retrieved from the resampled velocities using the original and improved GVTD algorithms (Table 1). Figure 3a and b show the Doppler velocity observed by the KAMX radar and the Doppler velocity projected from the dual Doppler analysis using the 1855 - 1940 UTC aircraft data as an example. Figure 3c and d show the reflectivity field from the KAMX radar observation and dual-Doppler analysis respectively. The single Doppler observations have much more missing data in the eye and the moat due to the reduced sensitivity to weak echoes at longer range from the radar. Additionally, the maximum Doppler velocity of single Doppler observations is not collocated with the maximum Doppler velocity of the resampled dual Doppler analysis. This discrepancy is believed to be due to temporal aliasing from the extended sampling period of the aircraft pass compared to the ground-based scanning. The issue of temporal aliasing of airborne Doppler analysis will be discussed in more detail in section 4.2. Despite the aliasing, the dual Doppler analysis provides a relatively complete, consistent wind field and can reasonably be assumed as the "truth" for the purposes of algorithm evaluation.

Figure 4 displays the results from the improved GVTD algorithm compared to the original GVTD algorithm and the "true" wavenumber 0 (axisymmetric) tangential wind derived from the four dual-Doppler analyses. The green dashed line (hereafter optimal solution) shows the improved GVTD retrieved axisymmetric tangential wind ($V_T C_0$) when all the terms are known. This optimal retrieval from the resampled $V_d D/R_T$ from the dual Doppler analysis using Eq. ~~16~~ 17 has the least deviation from the "truth" (black line) in general. When the storm motion is removed from the $V_T C_0$ retrieval (blue dashed line, hereafter optimal but without storm motion) the axisymmetric wind in the inner eyewall (between 10 and 30 km) does not differ significantly from the "truth". As the radius increases, the storm motion term becomes more important to the retrieval of wavenumber 0 tangential wind. Between the radius of 55 to 65 km the impact of neglecting the storm motion term can be up to 3-4 $\mathrm{m\,s^{-1}}$. In the optimal retrieval, all terms in Eq. ~~16~~ 17 are known, but in practice, the retrieved Fourier coefficients are underdetermined and a closure assumption is required to retrieve $V_T C_0$, typically by neglecting the cross-beam mean wind and asymmetric radial wind. The orange line (hereafter original GVTD) in Fig. 4 shows the result of the original GVTD algorithm invoking this closure assumption where only the ~~B1 and B3~~ B_1 and B_3 coefficients are used to retrieve $V_T C_0$. The red line (hereafter improved GVTD) shows the improvement to the GVTD algorithm by adding in the storm motion terms, while still invoking the necessary closure assumption. The deviations from the "truth" caused by the closure assumption occur at different radii depending on the aircraft pass, suggesting that the neglected terms have different magnitudes in different parts of the storm. For example, in pass 1 the deviations are most pronounced from 55 - 70 km radius, while in pass 4 the deviations are most pronounced from 15 - 25 km radius.

Root-mean-square (RMS) differences of the above $V_T C_0$ solutions and integrated perturbation pressure deficit (optimal, optimal but without storm motion, original GVTD and improved GVTD algorithms) averaged over the four passes are shown in Table 3. ~~The~~ For RMS difference of $V_T C_0$, the optimal solution has the least deviation from the "truth". Including the storm motion terms decreases the RMS differences about $0.8\,\mathrm{m\,s^{-1}}$ in both optimal versus optimal without storm motion and improved GVTD versus original GVTD. Interestingly, RMS difference of improved GVTD algorithm has a similar magnitude as the optimal solution but without storm motion, suggesting that the influence from storm motion herein is similar as neglecting terms in Eq. ~~16~~17.

The perturbation pressure deficit is integrated from r = 10 to 70 km using the gradient wind balance equation (Lee et al., 2000). The integrated perturbation pressure deficit retrievals from different methods agree well with the "truth" ($\sim$ 1 mb RMS in general). Similar as the results of RMS difference of $V_T C_0$, including the storm motion terms decreases the RMS differences about 0.2 mb. The RMS difference of improved GVTD algorithm from the single Doppler retrieval has the least deviation from the "truth", suggesting that the perturbation pressure deficit derived from the single Doppler observations has high fidelity.

The $V_T C_0$ retrieved by the original (orange dots) and improved (red dots) GVTD algorithm from the KAMX observations alone (Fig. 3a) are also shown in Fig. 4. The axisymmetric tangential winds retrieved from ~~KAMX~~ the KAMX radar alone are in generally good agreement with the winds from the dual Doppler analyses. As in the dual Doppler retrieval, the storm motion term has relatively small impact on the retrieval in the inner eyewall because R/R_T is small. The deviation between the retrievals becomes larger beyond the radius of 40 km, but the improved GVTD algorithm is generally more consistent with

the "truth" compared to the original GVTD algorithm. RMS differences show a reduction $0.4\,\mathrm{m\,s^{-1}}$ between the original and improved GVTD algorithms compared to the "truth" (Table 3). ~~The~~

A nonparametric Wilcoxon signed-rank test is conducted to test the null hypothesis that two paired sets of the RMS differences derived from the original and improved GVTD algorithms are drawn from the same distribution. The RMS difference between the original and improved GVTD algorithms is statistically significant with a p value < 0.001 using both the projected dual-Doppler winds and single-Doppler velocities, indicating that we can reject the null hypothesis at the 1% significance level (99% confidence). The statistics suggest that the RMS differences distribution of wavenumber 0 tangential wind retrieved from the original GVTD algorithm are likely to be larger than those from the improved GVTD method. While it is a relatively small reduction in the RMS difference in the current case, the statistically significant difference in this algorithm error contributes to an overall reduction in the total error from instrument, algorithm, and sampling contributions. The comparison demonstrates that the inclusion of the storm motion has better consistency of the wavenumber 0 tangential wind intensity with the dual-Doppler reference solution, and that the improved GVTD technique can provide insightful information about TC kinematic structure from ground-based single Doppler radar data.

4.2 Asymmetric wind retrievals

Both Lee et al. (1999) and Jou et al. (2008) have tested the GBVTD and GVTD techniques respectively with analytic datasets and confirmed the accuracy of these two methods. Murillo et al. (2011) further assessed the ability of GBVTD to retrieve low-wavenumber wind structure by comparing simultaneous single Doppler and dual-Doppler retrievals in Hurricane Danny (1999) using ground-based radar observations. However, no previous studies to the authors' knowledge have conducted a detailed comparison of the Fourier decomposition of the wind field between the ground-based single Doppler and airborne dual-Doppler wind retrievals. We have already shown that wavenumber 0 tangential wind from the dual Doppler analyses can be accurately retrieved by the GVTD-improved algorithm in section 4.1. With the confidence of the performance of the GVTD technique, the next step is to examine the low-wavenumber structure and applicability of a steady-state assumption of the dual Doppler analysis.

Figure 5a displays V_dD/R_T on a ring at the RMW (18 km) derived from the dual Doppler and single Doppler analyses. For clarity, we use the term "harmonics" to refer to Fourier decomposition in V_dD/R_T around the ring, and "wavenumbers" to refer to the components of tangential wind which are constructed from combinations of the observed Doppler harmonics. V_dD/R_T constructed from both analyses are dominated by a single harmonic pattern with very similar magnitude. Nevertheless, a small difference of V_dD/R_T pattern between the two analyses is evident. The discrepancies of the pattern and magnitude suggest that higher harmonics of the V_dD/R_T coefficients are different.

Figure 5b shows the residuals after the subtraction of harmonics 0 and 1 components from the total V_dD/R_T, with the harmonic 2 components of V_dD/R_T highlighted. The residuals include the harmonic 2 and higher components of V_dD/R_T. The residuals from the single Doppler analysis (light red line) are dominated by a wavenumber 2 component, while the residuals from the dual Doppler analysis (light green line) are without a clear pattern. The peak value of the residual from the single Doppler analysis is $8\,\mathrm{m\,s^{-1}}$, but the peak value of the residual from the dual Doppler analysis is about $3\,\mathrm{m\,s^{-1}}$. To quantitatively

compare the two retrievals, Table 4 shows the retrieved magnitude of harmonics 0 - 3 around the RMW. The magnitude of harmonics 0, 1, and 3 are similar at the RMW for the two analyses with around $1\,\mathrm{ms}^{-1}$ deviation. The similarity in harmonic 1 is primarily responsible for the similarity in the wavenumber 0 tangential wind (Fig. 4). Harmonic 2 shows a much larger deviation of $6\,\mathrm{ms}^{-1}$, resulting in different wavenumber 1 tangential wind retrievals.

Figure 6 shows the harmonics of $V_d D/R_T$ as a function of radius for the resampled dual Doppler wind field (green dashed line) and single Doppler observations (red dots). Note that the ordinate on each panel is different due to the varying magnitudes of each coefficient. The deviations of A_0, A_1 and B_1 coefficients ~~are roughly consistent~~ between the two analyses within the eyewall region (15 - 25 km) ~~with small deviations~~ are less than $2\,\mathrm{ms}^{-1}$. The deviations in A_0, A_1 and B_1 coefficients are larger from the eye to the inner edge of the eyewall (10 - 15 km) and outside of the eyewall region (beyond 25 km), but generally have a similar magnitude. On the other hand, larger discrepancies are apparent with A_2 and B_2. A_2 is similar between 10 to 20 km, but has a large $7\,\mathrm{ms}^{-1}$ difference outside 20 km. B_2 is different at nearly all radii, with up to $7\,\mathrm{ms}^{-1}$ differences. The different amplitudes of A_2 and B_2 indicate that the retrieved wavenumber 1 tangential wind phase and magnitude are inconsistent (Eq. 19). Discrepancies are also evident in the A_3 and B_3 coefficients, indicating inconsistencies in the retrieved wavenumber 2 tangential wind phase and magnitude as well. Since the axisymmetric radial wind is influenced by the harmonic 2 and 3 components (Eq. 20), we cannot fully validate the axisymmetric radial wind retrieval with the current dataset. The evaluation for the accuracy of the axisymmetric radial wind retrieval is not included in this study.

We hypothesize that the discrepancies of retrieved wavenumber 1 and 2 tangential winds are due to the steady state assumption in the dual Doppler ~~analysis. A~~ wind synthesis into one snapshot. Two different types of sampling errors in effect arise from the steady state assumption ~~is not applicable when~~ – the first is due to the time lag between fore and aft beams, and the second is due to the length of time used to composite the multi-Doppler into a single snapshot. While both produce some errors, the latter is more consequential when considering the temporal evolution of the phenomena is faster than the period of data collection~~.~~, resulting in evolution over the flight pass. The "local" wind may be correct, but the overall structure is distorted by collapsing to a single time. For example, the propagation velocity of a wavenumber 2 vortex Rossby wave (VRW) is half of the symmetric tangential wind velocity (Lamb, 1932; Guinn and Schubert, 1993; Kuo et al., 1999). A propagating wavenumber 2 asymmetry could then alias onto other wavenumbers, contributing to a discrepancy in wavenumber 1 tangential wind.

To test the hypothesis, the phases of maximum wavenumber 1 and wavenumber 2 tangential winds retrieved from the 5-minute single Doppler observations are examined in Fig. 7 for the temporal evolution during the first flight pass from 1907 to 1940 UTC. The amplitude and phase (Eqs. 18 and 19) of wavenumber 1 and 2 tangential winds are denoted in polar coordinates by the radius and azimuth, respectively. The wavenumber 1 tangential wind (Fig. 7a) generally stayed unchanged throughout the first pass with a magnitude between 8 and $12\,\mathrm{ms}^{-1}$ and phase to the E to NE (same as the wavenumber 1 reflectivity, not shown here). Environmental vertical wind shear derived from the Statistical Hurricane Intensity Prediction Scheme dataset (SHIPS) points to the northeast direction with a magnitude of $7\,\mathrm{ms}^{-1}$, suggesting that the wavenumber 1 distribution is forced by the vertical wind shear to be consistently in the downshear-right quadrant.

The wavenumber 2 tangential wind (Fig. 7b) propagated cyclonically during the flight pass (same as the wavenumber 2 reflectivity, not shown here) with a magnitude up to $7\,\mathrm{ms}^{-1}$. The propagation of the wavenumber 2 tangential wind is estimated

to be 285 degrees from 1907 to 1940 UTC, which is $35\,\mathrm{m\,s^{-1}}$, or 63% of $V_{T\,max}$. The propagation of the wavenumber 2 tangential wind is roughly consistent with linear VRW theory (Kuo et al., 1999; Cha et al., 2020).

According to the single Doppler analysis, the wavenumber 2 VRW propagated approximately 43 degrees every five minutes on average. The wavenumber 2 maximum amplitudes were located in the NE and SW quadrants as the P3 approached the inner eyewall from the SW (Fig. 2), such that the TDR would see the maximum component in the SW eyewall. The VRW rotated cyclonically as the P3 crossed the 36 km diameter eye at $120\,\mathrm{m\,s^{-1}}$, such that by the time the P3 exited the eyewall the radar would begin to see the wavenumber 2 wind minimum on the NE side. The SW maximum and NE minimum would then appear as a wavenumber 1 component under a steady state assumption. The analysis supports our hypothesis that the propagation of wavenumber 2 tangential wind is aliased onto the steady wavenumber 1 component, resulting in a reduced amplitude and a phase shift in A_2 and B_2 in the dual Doppler analysis.

The above analysis suggests that both the dual Doppler and single Doppler analysis have strengths and weaknesses. The retrieved wavenumber 0 component of tangential wind has been shown to be comparable between an airborne dual Doppler wind synthesis and single Doppler retrieval due to the fact that a steady state assumption for one flight pass is usually valid to apply to the axisymmetric circulation. The axisymmetric kinematic structure of Hurricane Matthew revealed in the dual Doppler analysis is consistent with the single Doppler retrievals across multiple aircraft passes (Cha, 2018). However, the steady-state assumption ~~is not~~ may not be applicable with more rapidly evolving features, such as convective bursts, rotation of mesovortices, and propagation of a wavenumber 2 or higher VRWs. The evolution during the aircraft pass could potentially impact the asymmetric reflectivity and wind structure retrieval from a dual or multi-Doppler analysis due to temporal aliasing. On the other hand, dual Doppler analysis can retrieve high-quality and detailed three-dimensional structure, whereas a ground-based single Doppler radar retrieval is often limited by spatial aliasing and the observing distance from the radar to TC. Nevertheless, the analyses presented herein demonstrate that complementary information can be retrieved from both single and dual Doppler retrievals.

4.3 An idealized experiment with a propagating wavenumber 2 asymmetry

To further test our hypothesis, we performed an idealized experiment to sample a rotating wavenumber 2 asymmetry by an aircraft with a realistic scanning strategy, similar to that first presented by Bell et al. (2007). The idealized framework allows for minimization of instrument and algorithm errors in order to isolate the sampling error due to the steady-state assumption. The simulated aircraft penetrates the TC "eyewall" at 120 m s^{-1} airspeed on a south to north flight track, which is a typical straight-line flight track during NOAA P3 operational reconnaissance. The radar has "perfect" FAST scanning with no instrument error and ideal geometry from the straight flight track, such that a steady-state wind field can be retrieved with minimal error (not shown). The TC wind field is a symmetric Rankine vortex with a 20 km RMW and V_{max} of $50\,\mathrm{m\,s^{-1}}$, representative of a strong mature TC, with an added propagating wavenumber 2 linear Rankine edge wave with an epsilon of 3 km corresponding to an amplitude of 7.1 m s^{-1} as in Lee et al. (2006). The initial phase of the asymmetry is oriented from east to west, and it rotates around the RMW cyclonically at 1/2 V_{max}. The simulated aircraft takes 22 minutes to cross the 160 km distance through the storm, during which time the wavenumber 2 asymmetry rotates to have a north-south orientation.

The time-mean phase of the asymmetry is therefore 45 degrees, oriented from southwest to northeast over the course of the sampling period.

Figure 8a shows the derived tangential wind for a wavenumber 2 rotation during the flight pass. The overall magnitude of the wind field is close to the prescribed time-mean structure but is distorted, suggesting temporal aliasing from the extended sampling period of the aircraft pass due to the propagation of the wavenumber 2 asymmetry. Figure 8b - d shows the retrieved wavenumber 1, 2 and 3 tangential wind fields from the Fourier decomposition. Although only a wavenumber 2 component is prescribed in the experiment, the retrieved wavenumber 1 and 3 components are up to 1.5 - 2 m s^{-1}. The orientation of the flow is close to the "true" time-mean structure shown in black contours, and the Fourier wavenumber 2 component has the generally correct phase. We note that the amplitude of the wavenumber 2 component correctly changes sign at the RMW due to the construction of a pure vorticity wave and is consistent with the prescribed flow and phase. The exact asymmetry retrieved depends to a large extent on the specifics of the flight track. However, we note that over the 22 minute period, a ground-based single Doppler retrieval would see the storm ∼4 times with different phase orientations of the asymmetry (not shown). While idealized, this experiment provides further evidence that the steady-state assumption to synthesize the data into one snapshot with the presence of evolving features could result in temporal aliasing and result in potential misinterpretation of the asymmetric flow field.

5 Conclusions

Tropical cyclone (TC) wind retrieval techniques from Doppler radar observations are salient to identify the convective and kinematic structure and evolution of TCs. ~~Previous studies have used the ground-based velocity track display (GBVTD) (Lee et al., 1999; Lee and Marks, 2000; Lee and Bell, 2007; Zhao et al., 2008) or the generalized velocity track display (GVTD) (Jou et al., 2008; Cha et al., 2020) techniques from single Doppler observations, and airborne dual-Doppler analysis (Bell et al., 2012; Cha, analyze TC intensity evolution, but no previous studies to the authors' knowledge have conducted a~~ The current study is believed to be the first detailed comparison of the retrieved wind field between ground-based single Doppler and airborne dual-Doppler wind ~~retrievals~~techniques. Hurricane Matthew (2016) was observed by the polarimetric Next Generation Weather Radar (NEXRAD) in Miami (KAMX) and NOAA P-3 airborne radar near the coast of Florida for several hours, providing a novel opportunity to evaluate and compare single and dual Doppler wind retrieval techniques for TC flows.

Jou et al. (2008) has shown that the GVTD technique improves the capability of the GBVTD and can retrieve a subset of the wind field from a single ground-based Doppler radar under the assumption of nearly axisymmetric rotational wind. Here we present an improved technique that mitigates errors due to storm motion, which yields a more accurate estimation of mean wind, wavenumber 0 tangential and radial winds. The aliasing of unresolved wind components from the single Doppler measurements remains, so another closure assumption for the GVTD technique is needed to improve the accuracy of the retrieval in the future. In addition to the wind improvements, the GVTD-simplex centers follow more closely to the dynamic centers compared to GBVTD-simplex centers due to the more accurate estimation of axisymmetric tangential wind. However, the GVTD-simplex centers are still ~~varying~~ variable and not fully consistent ~~with different radar~~ between retrievals from different radars (such as

KAMX vs. KMLB, and KMLB vs. KJAX). The dynamic centers herein are shown to be qualitatively and quantitatively better than the simplex center, suggesting further improvement is needed in the technique. Nevertheless, the improvement of TC wind estimation from single Doppler radar presented herein can be useful in deducing storm structure for research purposes and assimilating real-time TC intensity and structure for forecasts (Zhao et al., 2012).

The strengths and weaknesses of different platform observing capabilities and retrieval techniques for TC wind fields are discussed in this study. The full three-dimensional wind field from airborne radar fore-aft pseudo-dual Doppler scanning can be retrieved by a spline-based technique called SAMURAI, but is shown to have errors due to temporal aliasing from the non-simultaneous Doppler measurements when the temporal evolution of the phenomena is faster than the period of data collection. Single Doppler wind retrieval by the GVTD technique can be obtained at a 5-minute interval, but spatial aliasing remains due to the limited measurements from only radial direction of the radar beam. A comparison between the two techniques shows that the retrieved axisymmetric (wavenumber 0) component of tangential winds are generally comparable between the two techniquesafter the improvements to GVTD retrievals, due to the fact that a steady state assumption for one flight pass (30-60 minutes) is usually valid to apply to the axisymmetric circulation, and the improved GVTD technique improves the accuracy of the retrieval. Fourier decomposition of asymmetric kinematic and convective structure shows more discrepancies between the two techniques due to spatial and temporal aliasing in the retrievals. The propagation of wavenumber 2 tangential wind is found to be aliased onto the steady wavenumber 1 component retrieved by the dual Doppler analysis, causing a reduced amplitude and phase shift of wavenumber 1 tangential wind. The steady-state assumption for low-wavenumber structure retrievals from pseudo-dual Doppler analysis is not may not be applicable with the presence of rapidly evolving features, and the temporal evolution within one during a flight pass should be considered. On the other hand, the steady-state assumption is less severe for single Doppler wind retrievals, and the rapidly evolving phenomena, such as vortex Rossby waves, have been documented by several studies using the single Doppler observations (Corbosiero et al., 2006; Cha et al., 2020). The analyses presented herein demonstrate that complementary information can be retrieved from both single and dual Doppler retrievals. Future work on the time-dependent analysis of asymmetric structure in dual Doppler retrieval and asymmetric flow closure assumptions in single Doppler retrieval are required to reconcile differences in retrieved TC structure.

Code and data availability. The underlying Julia code used for analysis in this study is available from the author upon request. The Vortex Objective Radar Tracking And Circulation (VORTRAC) and SAMURAI software are part of the Lidar Radar Open Software Environment (LROSE) and are available on the web: http://lrose.net. The data used in this paper are available through zenodo: https://doi.org/10.5281/zenodo.4427194.

Author contributions. The study was designed by both authors. TC carried out the analysis and made the figures supervised by MB. TC wrote the manuscript with contributions from MB.

Competing interests. The authors declare that they have no conflict of interest.

Acknowledgements. This research was supported by National Science Foundation award OAC-1661663. We would like to thank NOAA Aircraft Operations Center and the Hurricane Research Division of the Atlantic Oceanographic and Meteorological Laboratory for collecting the airborne tail Doppler radar data used for this study, and the National Weather Service for the ground-based radar data.

References

Bell, M. M.: nsf-lrose/lrose-blaze: lrose-blaze-20190105, https://doi.org/10.5281/zenodo.2532758, 2019.

Bell, M. M., Lee, W.-C., Houze, R. A., Smull, B. F., and Marks, F. D.: Circular Flight Tracks for Deducing Tropical Cyclone Inner-core Structure Using Airborne Doppler Radar, 33rd Conference on Radar Meteorology, Cairns, Australia, 6-10 August 2007 [poster], 2007.

Bell, M. M., Montgomery, M. T., and Lee, W.-C.: An axisymmetric view of concentric eyewall evolution in Hurricane Rita (2005), J. Atmos. Sci., 69, 2414–2432, https://doi.org/10.1175/JAS-D-11-0167.1, 2012.

Bell, M. M., Lee, W.-C., Wolff, C. A., and Cai, H.: A Solo-based automated quality control algorithm for airborne tail Doppler radar data, J. Appl. Meteor. Climatol., 52, 2509–2528, https://doi.org/10.1175/JAMC-D-12-0283.1, 2013.

Cha, T.-Y.: Eyewall Replacement Cycle of Hurricane Matthew (2016) observed by Doppler radars, M. S. Thesis, p. Colorado State University, 2018.

Cha, T.-Y., Bell, M. M., Lee, W.-C., and DesRosiers, A. J.: Polygonal Eyewall Asymmetries During the Rapid Intensification of Hurricane Michael (2018), Geophys. Res. Lett., 47, e2020GL087 919, https://doi.org/https://doi.org/10.1029/2020GL087919, 2020.

Chan, J. C.: An observational study of the physical processes responsible for tropical cyclone motion, J. Atmos. Sci., 41, 1036–1048, https://doi.org/10.1175/1520-0469(1984)041<1036:AOSOTP>2.0.CO;2, 1984.

Chan, J. C. and Gray, W. M.: Tropical cyclone movement and surrounding flow relationships, Mon. Wea. Rev., 110, 1354–1374, https://doi.org/10.1175/1520-0493(1982)110<1354:TCMASF>2.0.CO;2, 1982.

Chen, X., Zhao, K., Lee, W.-C., Jong-Dao Jou, B., Xue, M., and Harasti, P. R.: The Improvement to the Environmental Wind and Tropical Cyclone Circulation Retrievals with the Modified GBVTD (MGBVTD) Technique, J. Appl. Meteor. Climatol., 52, 2493–2508, https://doi.org/10.1175/JAMC-D-13-031.1, 2013.

Corbosiero, K. L., Molinari, J., Aiyyer, A. R., and Black, M. L.: The structure and evolution of Hurricane Elena (1985). Part II: Convective asymmetries and evidence for vortex Rossby waves, Mon. Wea. Rev., 134, 3073–3091, https://doi.org/10.1175/MWR3250.1, 2006.

Crum, T. D., Saffle, R. E., and Wilson, J. W.: An Update on the NEXRAD Program and Future WSR-88D Support to Operations, Wea. Forecasting, 13, 253 – 262, https://doi.org/10.1175/1520-0434(1998)013<0253:AUOTNP>2.0.CO;2, 1998.

Gamache, J. F., Marks, F. D., and Roux, F.: Comparison of Three Airborne Doppler Sampling Techniques with Airborne In Situ Wind Observations in Hurricane Gustav (1990), J. Atmos. Oceanic Technol., 12, 171 – 181, https://doi.org/10.1175/1520-0426(1995)012<0171:COTADS>2.0.CO;2, 1995.

Griffin, J. S., Burpee, R. W., Marks, F. D., and Franklin, J. L.: Real-time airborne analysis of aircraft data supporting operational hurricane forecasting, Wea. Forecasting, 7, 480–490, https://doi.org/10.1175/1520-0434(1992)007<0480:RTAAOA>2.0.CO;2, 1992.

Guinn, T. A. and Schubert, W. H.: Hurricane Spiral Bands, Journal of the Atmospheric Sciences, 50, 3380–3403, https://doi.org/10.1175/1520-0469(1993)050<3380:HSB>2.0.CO;2, 1993.

Harasti, P. R., McAdie, C. J., Dodge, P. P., Lee, W.-C., Tuttle, J., Murillo, S. T., and Marks, F. D.: Real-Time Implementation of Single-Doppler Radar Analysis Methods for Tropical Cyclones: Algorithm Improvements and Use with WSR-88D Display Data, Wea. Forecasting, 19, 219 – 239, https://doi.org/10.1175/1520-0434(2004)019<0219:RIOSRA>2.0.CO;2, 2004.

Hildebrand, P. H. and Mueller, C. K.: Evaluation of Meteorological Airborne Doppler Radar. Part I: Dual-Doppler Analyses of Air Motions, J. Atmos. Oceanic Technol., 2, 362 – 380, https://doi.org/10.1175/1520-0426(1985)002<0362:EOMADR>2.0.CO;2, 1985.

Hildebrand, P. H., Walther, C., and Frush, C.: The NCAR Electra Doppler radar, in: Part I: Evaluation of scientific needs. Preprints, 23rd Conf. on Radar Meteorology, Snowmass, CO, Amer. Meteor. Soc, pp. 147–150, 1986.

Hildebrand, P. H., Walther, C. A., Frush, C. L., Testud, J., and Baudin, F.: The ELDORA/ASTRAIA airborne Doppler weather radar: goals, design, and first field tests, Proceedings of the IEEE, 82, 1873–1890, https://doi.org/10.1109/5.338076, 1994.

Houze, Robert A., J.: Clouds in Tropical Cyclones, Mon. Wea. Rev., 138, 293–344, https://doi.org/10.1175/2009MWR2989.1, 2010.

Jorgensen, D., Matejka, T., and DuGranrut, J.: Multi-beam techniques for deriving wind fields from airborne Doppler radars, Meteor. Atmos. Phys., 59, 83–104, https://doi.org/10.1007/BF01032002, 1996.

Jorgensen, D. P., Hildebrand, P. H., and Frush, C. L.: Feasibility Test of an Airborne Pulse-Doppler Meteorological Radar, J. Appl. Meteor. Climatol., 22, 744 – 757, https://doi.org/10.1175/1520-0450(1983)022<0744:FTOAAP>2.0.CO;2, 1983.

Jou, B. J.-D., Deng, S.-M., and Chang, B.: Determination of typhoon center and radius of maximum wind by using Doppler radar, Atmos. Sci, 24, 1–24, 1996.

Jou, B. J.-D., Lee, W.-C., Liu, S.-P., and Kao, Y.-C.: Generalized VTD retrieval of atmospheric vortex kinematic structure. Part I: Formulation and error analysis, Mon. Wea. Rev., 136, 995–1012, https://doi.org/10.1175/2007MWR2116.1, 2008.

Koch, S. E., desJardins, M., and Kocin, P. J.: An Interactive Barnes Objective Map Analysis Scheme for Use with Satellite and Conventional Data, J. Appl. Meteor. Climatol., 22, 1487 – 1503, https://doi.org/10.1175/1520-0450(1983)022<1487:AIBOMA>2.0.CO;2, 1983.

Kuo, H.-C., Williams, R., and Chen, J.-H.: A possible mechanism for the eye rotation of Typhoon Herb, J. Atmos. Sci., 56, 1659–1673, https://doi.org/10.1175/1520-0469(1999)056<1659:APMFTE>2.0.CO;2, 1999.

Lamb, H.: Hydrodynamics, Cambridge university press, 1932.

Lee, W.-C. and Bell, M. M.: Rapid intensification, eyewall contraction, and breakdown of Hurricane Charley (2004) near landfall, Geophys. Res. Lett., 34, https://doi.org/10.1029/2006GL027889, 2007.

Lee, W.-C. and Marks, F. D.: Tropical cyclone kinematic structure retrieved from single-Doppler radar observations. Part II: The GBVTD-simplex center finding algorithm, Mon. Wea. Rev., 128, 1925–1936, https://doi.org/10.1175/1520-0493(2000)128<1925:TCKSRF>2.0.CO;2, 2000.

Lee, W.-C., Marks, F. D., and Carbone, R. E.: Velocity track display—A technique to extract real-time tropical cyclone circulations using a single airborne Doppler radar, J. Atmos. Oceanic Technol., 11, 337–356, https://doi.org/10.1175/1520-0426(1994)011<0337:VTDTTE>2.0.CO;2, 1994.

Lee, W.-C., Jou, B. J.-D., Chang, P.-L., and Deng, S.-M.: Tropical cyclone kinematic structure retrieved from single-Doppler radar observations. Part I: Interpretation of Doppler velocity patterns and the GBVTD technique, Mon. Wea. Rev., 127, 2419–2439, https://doi.org/10.1175/1520-0493(1999)127<2419:TCKSRF>2.0.CO;2, 1999.

Lee, W.-C., Jou, B. J.-D., Chang, P.-L., and Marks, F. D.: Tropical cyclone kinematic structure retrieved from single-Doppler radar observations. Part III: Evolution and structures of Typhoon Alex (1987), Mon. Wea. Rev., 128, 3982–4001, https://doi.org/10.1175/1520-0493(2000)129<3982:TCKSRF>2.0.CO;2, 2000.

Lee, W.-C., Marks, F. D., and Walther, C.: Airborne Doppler radar data analysis workshop, Bull. Amer. Meteor. Soc., 84, 1063–1075, 2003.

Lee, W.-C., Harasti, P. R., Bell, M. M., Jou, B. J.-D., and Chang, M.-H.: Doppler velocity signatures of idealized elliptical vortices, TAO: Terrestrial, Atmospheric and Oceanic Sciences, 17, 429, 2006.

Liou, Y.-C., Wang, T.-C. C., Lee, W.-C., and Chang, Y.-J.: The retrieval of asymmetric tropical cyclone structures using Doppler radar simulations and observations with the extended GBVTD technique, Mon. Wea. Rev., 134, 1140–1160, https://doi.org/10.1175/MWR3107.1, 2006.

Lorsolo, S. and Aksoy, A.: Wavenumber analysis of azimuthally distributed data: Assessing maximum allowable gap size, Mon. Wea. Rev., 140, 1945–1956, https://doi.org/10.1175/MWR-D-11-00219.1, 2012.

Marks, F. D. and Houze, R. A.: Airborne Doppler Radar Observations in Hurricane Debby, Bull. Amer. Meteor. Soc., 65, 569–582, https://doi.org/10.1175/1520-0477(1984)065<0569:ADROIH>2.0.CO;2, 1984.

Marks, F. D. and Houze, R. A.: Inner Core Structure of Hurricane Alicia from Airborne Doppler Radar Observations, J. Atmos. Sci., 44, 1296–1317, https://doi.org/10.1175/1520-0469(1987)044<1296:ICSOHA>2.0.CO;2, 1987.

Marks, F. D., Houze, R. A., and Gamache, J. F.: Dual-aircraft investigation of the inner core of Hurricane Norbert. Part I: Kinematic structure, J. Atmos. Sci., 49, 919–942, https://doi.org/10.1175/1520-0469(1992)049<0919:DAIOTI>2.0.CO;2, 1992.

Matejka, T. and Srivastava, R. C.: An Improved Version of the Extended Velocity-Azimuth Display Analysis of Single-Doppler Radar Data, J. Atmos. Oceanic Technol., 8, 453 – 466, https://doi.org/10.1175/1520-0426(1991)008<0453:AIVOTE>2.0.CO;2, 1991.

Murillo, S. T., Lee, W.-C., Bell, M. M., Barnes, G. M., Marks, F. D., and Dodge, P. P.: Intercomparison of Ground-Based Velocity Track Display (GBVTD)-Retrieved Circulation Centers and Structures of Hurricane Danny (1997) from Two Coastal WSR-88Ds, Monthly Weather Review, 139, 153–174, https://doi.org/10.1175/2010MWR3036.1, 2011.

Ray, P. S. and Stephenson, M.: Assessment of the Geometric and Temporal Errors Associated with Airborne Doppler Radar Measurements of a Convective Storm, J. Atmos. Oceanic Technol., 7, 206 – 217, https://doi.org/10.1175/1520-0426(1990)007<0206:AOTGAT>2.0.CO;2, 1990.

Reasor, P. D., Montgomery, M. T., Marks, F. D., and Gamache, J. F.: Low-wavenumber structure and evolution of the hurricane inner core observed by airborne dual-Doppler radar, Mon. Wea. Rev., 128, 1653–1680, https://doi.org/10.1175/1520-0493(2000)128<1653:LWSAEO>2.0.CO;2, 2000.

Shimada, U., Sawada, M., and Yamada, H.: Doppler Radar Analysis of the Rapid Intensification of Typhoon Goni (2015) after Eyewall Replacement, J. Atmos. Sci., 75, 143–162, https://doi.org/10.1175/JAS-D-17-0042.1, 2018.

Willoughby, H. E. and Chelmow, M. B.: Objective determination of hurricane tracks from aircraft observations, Mon. Wea. Rev., 110, 1298–1305, https://doi.org/10.1175/1520-0493(1982)110<1298:ODOHTF>2.0.CO;2, 1982.

Wood, V. T. and Brown, R. A.: Effects of radar proximity on single-Doppler velocity signatures of axisymmetric rotation and divergence, Mon. Wea. Rev., 120, 2798–2807, https://doi.org/10.1175/1520-0493(1992)120<2798:EORPOS>2.0.CO;2, 1992.

Zhao, K., Lee, W.-C., and Jou, B. J.-D.: Single Doppler radar observation of the concentric eyewall in Typhoon Saomai, 2006, near landfall, Geophys. Res. Lett., 35, https://doi.org/10.1029/2007GL032773, 2008.

Zhao, K., Xue, M., and Lee, W.-C.: Assimilation of GBVTD-retrieved winds from single-Doppler radar for short-term forecasting of super typhoon Saomai (0608) at landfall, Quart. J. Roy. Meteor. Soc., 138, 1055–1071, https://doi.org/10.1002/qj.975, 2012.

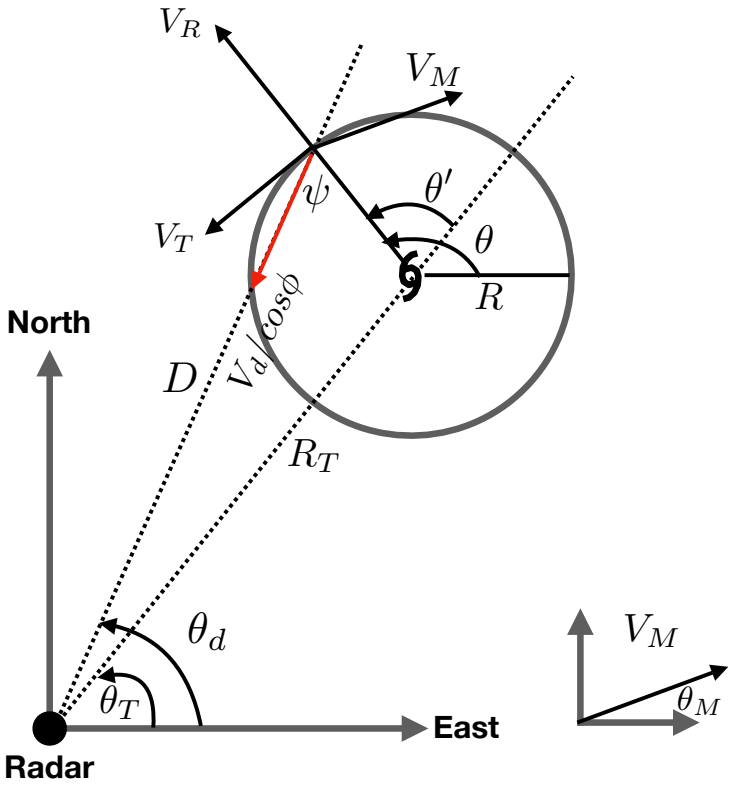

Figure 1. The geometry and symbols used in the formulation of GVTD (modified from Jou et al. (2008)). Red arrow denotes the Doppler velocity. Symbols are defined in the text.

Table 1. Details of aircraft missions and corresponded KAMX ground-based radar observation period for this study.

Radar analysis	Duration
P3	1855-1940 UTC 6 Oct 2016
P3	2020-2105 UTC 6 Oct 2016
P3	2145-2230 UTC 6 Oct 2016
P3	2305-2340 UTC 6 Oct 2016
KAMX	1907-0550 UTC 6-7 Oct 2016

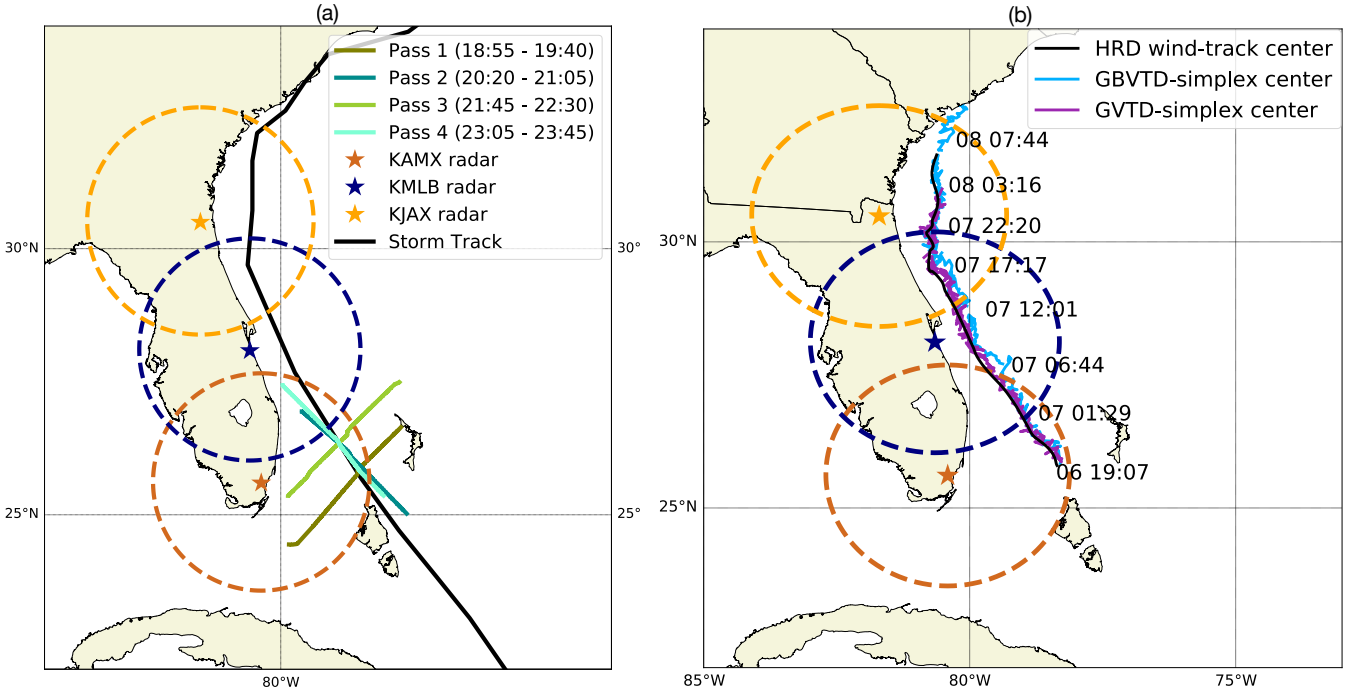

Figure 2. (a) Hurricane Matthew's ~~storm~~ center track from best track data (black line) and ~~the deployed observation instruments~~different radar and aircraft estimates. ~~Pass~~ Passes 1-4 denote the ~~passage~~ consecutive flight segments of ~~P-3 plane~~ the P3 aircraft across the cyclone on 6 October. Colored circles and stars represent the ground-based radar detecting range (230 km) and location of single Doppler radar respectively. (b) Comparison of Hurricane Matthew's track between HRD dynamic aircraft center (black line), GBVTD-simplex center (light blue line), and GVTD-simplex center (purple line). Colored circles and stars are the same as (a).

Table 2. The maximum allowable data gap determines the maximum wavenumber used in the least squares fit.

Wavenumber	Gap(^{o})
0	≤ 180
1	≤ 90
2	≤ 60

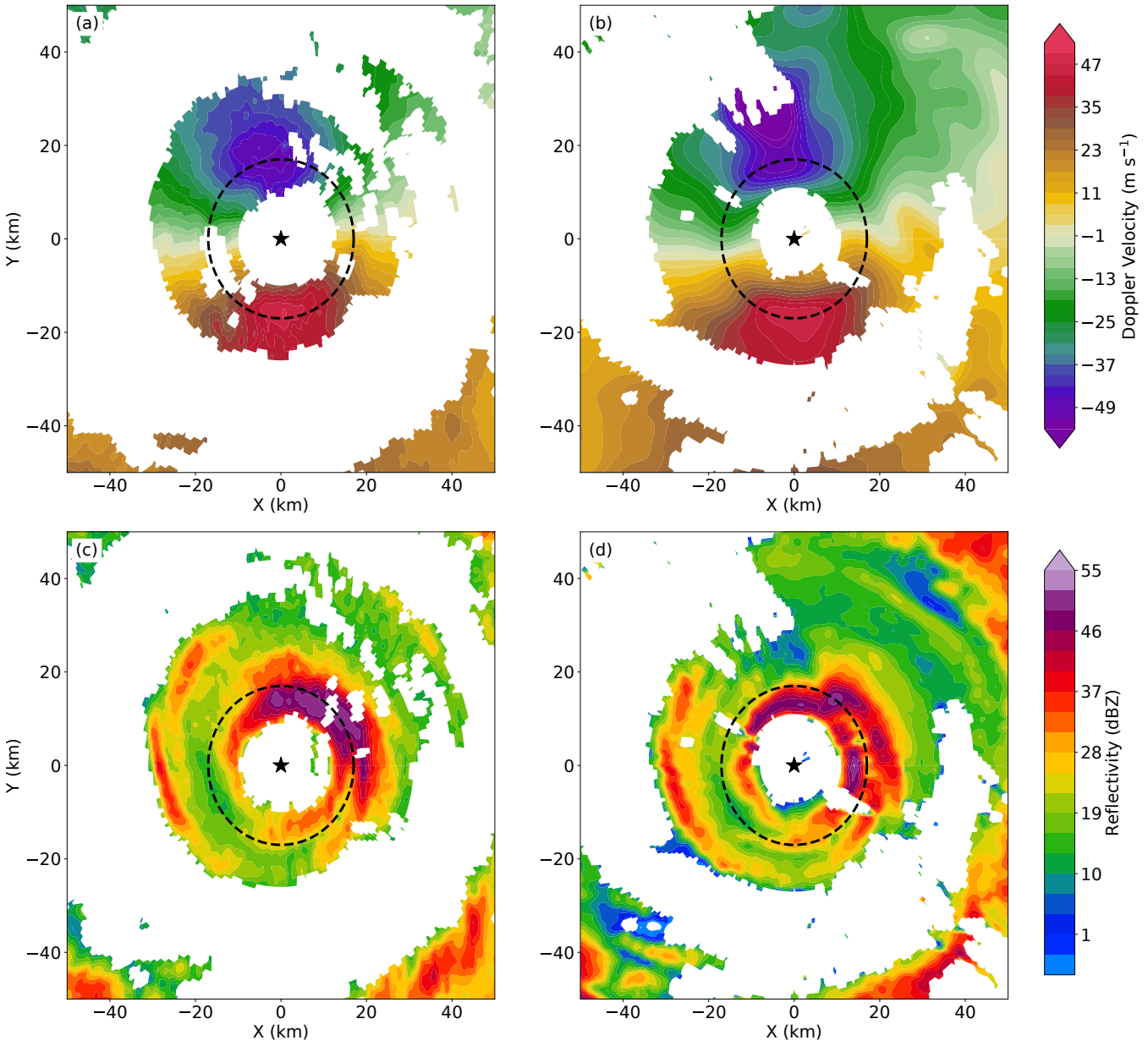

Figure 3. Doppler velocity at ~~z =~~ 4 km constant altitude (a) observed by the KAMX radar at 1921 UTC, and (b) resampled from the dual Doppler analysis synthesized from 1855 - 1940 UTC. Reflectivity at 4 km altitude (c) observed by the KAMX radar and (d) derived from the dual Doppler analysis. The timing of (c) and (d) are the same as (a) and (b), respectively. The black star denotes ~~KAMX radar location~~the TC center, and the dashed circle denotes the radius of maximum wind of 18 km.

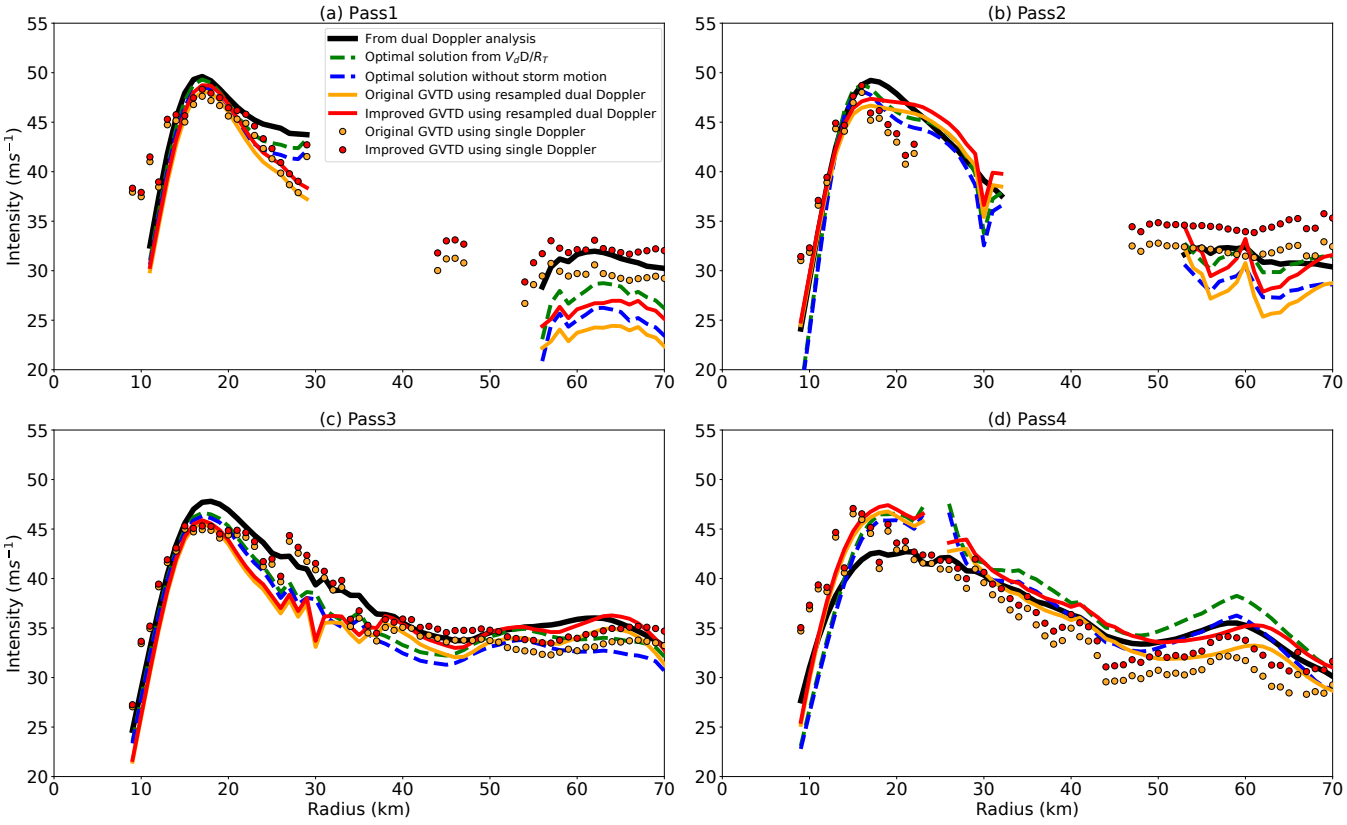

Figure 4. Wavenumber 0 tangential wind retrieved by various techniques at (a) Pass 1 from 1855 to 1940 UTC, (b) Pass 2 from 2020 to 2105 UTC, (c) Pass 3 from 2145 to 2230 UTC, (d) Pass 4 from 2305 to 2340 UTC. The retrievals are the Fourier decomposition of tangential wind from the dual Doppler analysis (black line), the Fourier decomposition of V_dD/R_T (green dashed line), the Fourier decomposition of V_dD/R_T without storm motion (blue dashed line), the original GVTD algorithm (orange line) ~~, the~~ and improved GVTD algorithm (red line) from the resampled dual Doppler analysis~~. Wavenumber 0 tangential wind retrieved by~~ , and the ~~single Doppler analysis from the~~ original GVTD algorithm (orange dot) ~~,~~ and improved GVTD algorithm (red dot) ~~. (a) Pass 1~~ from ~~1855 to 1940 UTC, (b) Pass 2 from 2020 to 2105 UTC, (c) Pass 3 from 2145 to 2230 UTC, (d) Pass 4 from 2305 to 2340 UTC~~the single Doppler observations.

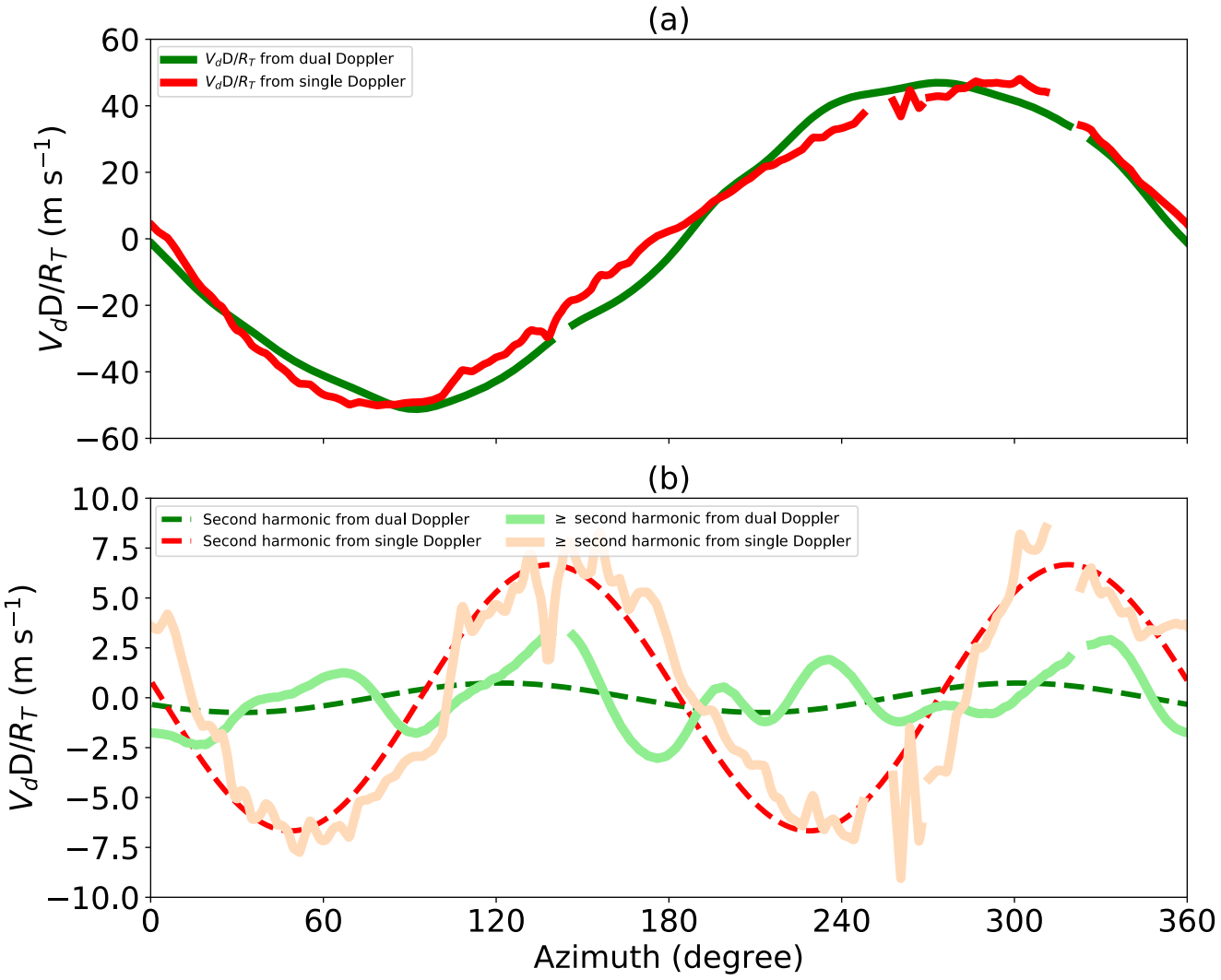

Figure 5. (a) Comparison of retrieved V_dD/R_T between the dual Doppler and single Doppler analyses at the RMW of 18 km. Green line denotes retrieved V_dD/R_T from the resampled dual Doppler analysis synthesized from 1855 - 1940 UTC, and red line denotes retrieved V_dD/R_T from the KAMX radar at 1921 UTC. (b) Comparison of retrieved ~~equal or greater than~~ second harmonic and higher components of V_dD/R_T between the dual Doppler and single Doppler analyses at the RMW. The solid line denotes the residuals of subtracting the harmonics 0 and 1 from V_dD/R_T. The dashed line represents the harmonic 2 of V_dD/R_T.

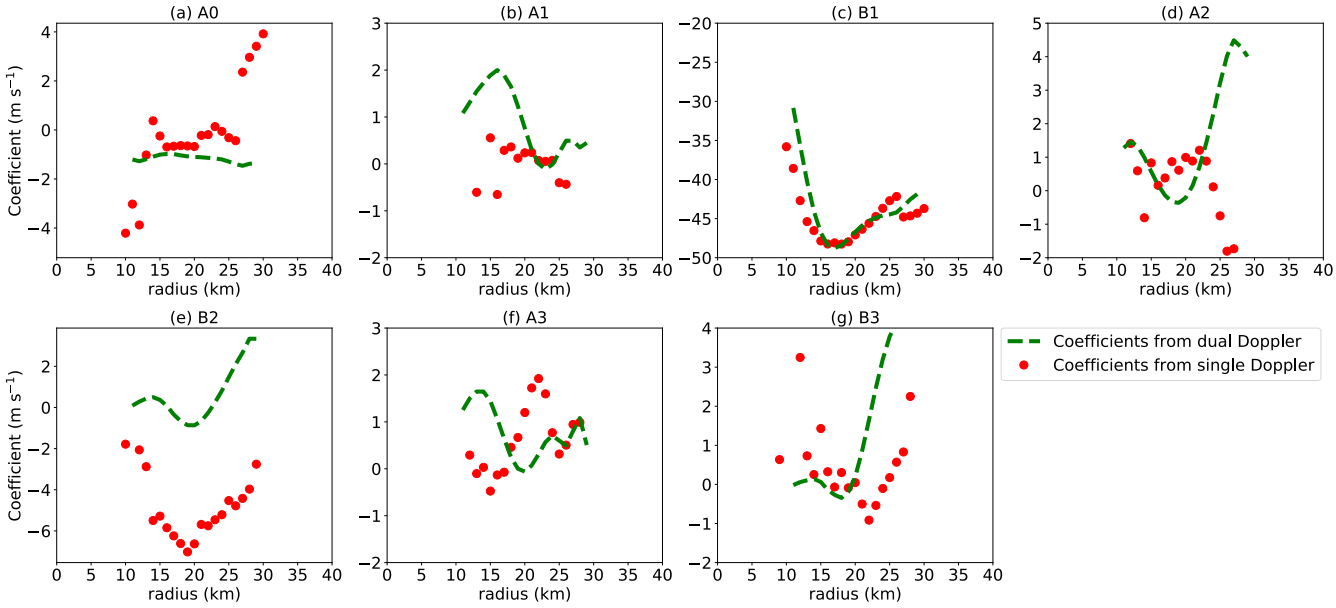

Figure 6. Comparison of $V_d D/R_T$ harmonics coefficients derived from the resampled ~~Doppler velocity of~~ dual Doppler ~~analysis~~ winds synthesized from 1855 - 1940 UTC using the improved GVTD technique (green dashed line), and single Doppler retrieval at 1921 UTC using the improved GVTD technique (red dot). (a) A_0 (to obtain $V_R C_0$ and $V_M cos(\theta_T - \theta_M)$) (b) A_1 (to obtain $V_R C_0$) (c) B_1 (to obtain $V_T C_0$) (d) A_2 (to obtain $V_R C_0$ and $V_T S_1$) (e) B_2 (to obtain $V_T C_1$) (f) A_3 (to obtain $V_R C_0$ and $V_T S_2$) (g) B_3 (to obtain $V_T C_0$ and $V_T C_2$)

Table 3. The averaged root mean squared error of the $V_T C_0$ and integrated perturbation pressure deficit retrieved from different methods described in Fig. 4 from the four flight passes and single Doppler radar observations. The errors are calculated from r = 10 - 70 km on z = 4 km.

~~Errors~~ RMSE	P-3 dual-Doppler				NEXRAD single Doppler	
	Optimal	Optimal but no storm motion	Origial GVTD	Improved GVTD	Origial GVTD	Improved GVTD
~~RMSE~~ $V_T C_0$ (m s^{-1})	1.49	2.37	3.17	2.3	2.81	2.46
Integrated perturbation pressure deficit (mb)	0.91	1.14	1.3	1.07	0.84	0.68

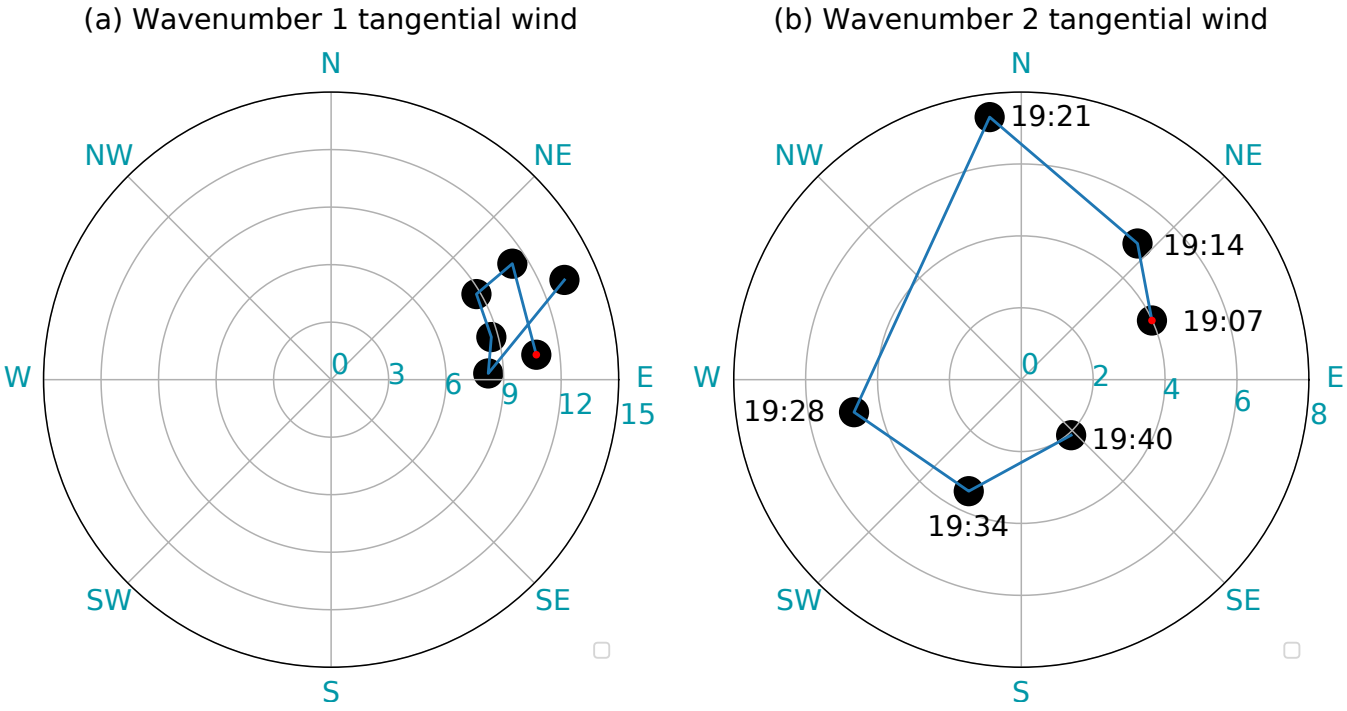

Figure 7. Azimuth and amplitude polar diagram of the temporal evolution of (a) maximum wavenumber 1 tangential wind amplitude and phase and (b) maximum wavenumber 2 tangential wind amplitude and phase in the inner eyewall (<18 km) derived from the GVTD single Doppler analysis from 1907 to 1940 UTC 6 October. The amplitude of the tangential wind component is denoted by the radius of each dot, with the phase denoted by the azimuth. The red dot in (a) and (b) indicates the starting time at 1907 UTC, and the temporal evolution follows the blue line.

Table 4. ~~The Fourier coefficient magnitude of wavenumber~~ $V_d D/R_T$ harmonics coefficients amplitude (harmonics 0 ~~, wavenumber 1 and wavenumber 2~~ to 3) retrieved ~~by~~ from the single Doppler and dual Doppler analyses.

Coefficient magnitude (m s^{-1})	Single Doppler retrieval	Dual Doppler retrieval
A_0	0.26	-1.08
$\sqrt{{A_1}^2 + {B_1}^2}$	46.29	47.61
$\sqrt{{A_2}^2 + {B_2}^2}$	7.05	0.93
$\sqrt{{A_3}^2 + {B_3}^2}$	0.67	0.19

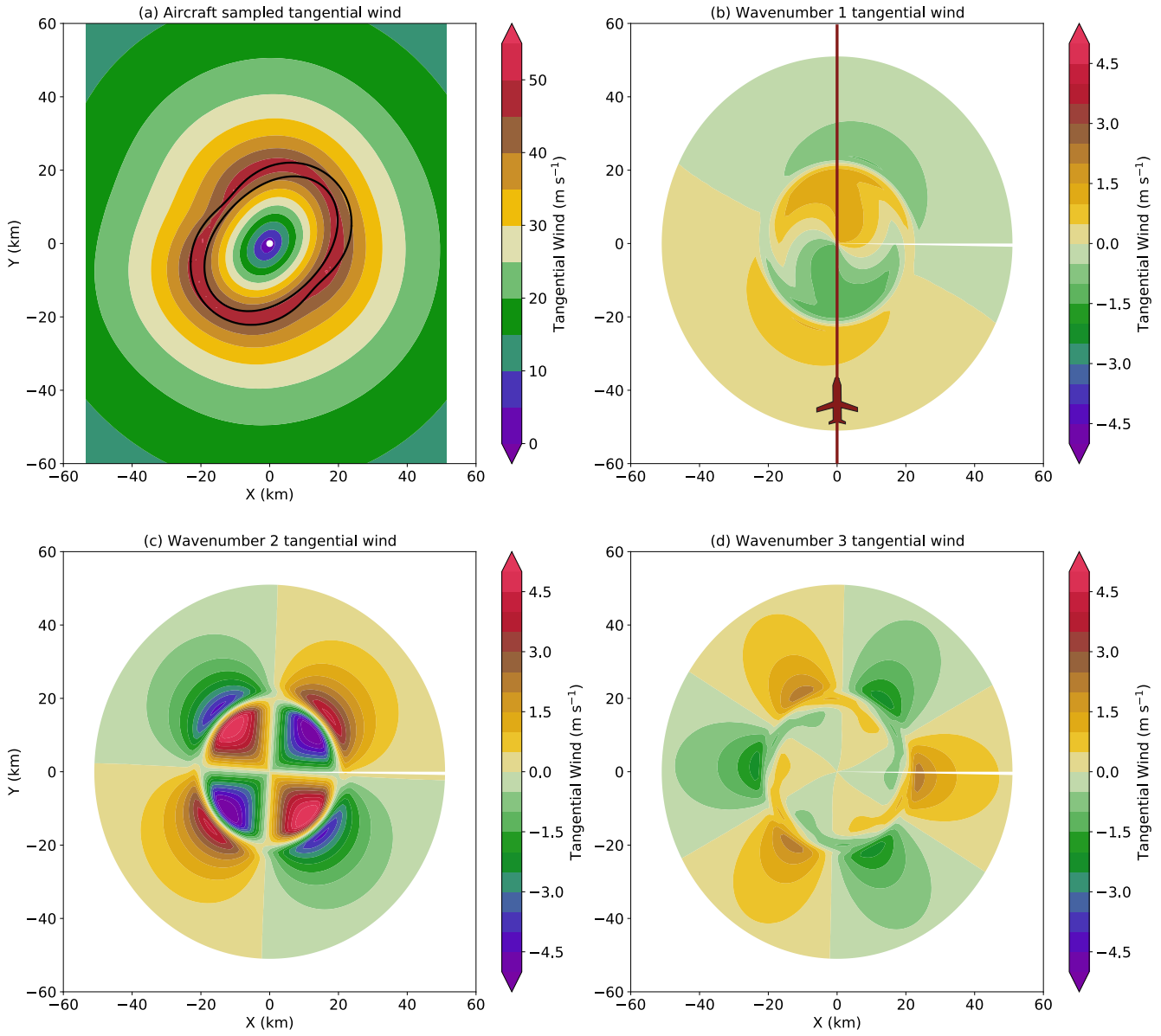

Figure 8. (a) Idealized dual-Doppler tangential wind speed retrieved from a straight flight pass through propagating wavenumber two asymmetry (color in m s^{-1}) and 45 m s^{-1} contour of prescribed, time-averaged wavenumber two in black. The initial phase of the propagating wavenumber 2 tangential wind is oriented from east to west and final phase is from north to south, resulting in a time-averaged southwest to northeast orientation. (b) Wavenumber 1 plus aircraft flight track from south to north, (c) Wavenumber 2, and (d) Wavenumber 3 tangential wind components retrieved by the Fourier decomposition of the tangential wind field shown in panel (a).